Conserved Biochemical Defenses Underpin Host Responses to Oomycete Infection in an Early Divergent Land Plant Lineage

AUTHORS:
Philip Carella[1], Anna Gogleva[1], David John Hoey[1], Anthony John Bridgen[1], Sara Christina Stolze[2], Hirofumi Nakagami[2], Sebastian Schornack*[1,3]

***Lead Contact & Corresponding Author** – Sebastian Schornack
(sebastian.schornack@slcu.cam.ac.uk)

AFFILIATIONS:
1 - University of Cambridge, Sainsbury Laboratory, Bateman Street, Cambridge, CB2 1LR, UK
2 - Max Planck Institute for Plant Breeding Research, Protein Mass Spectrometry Group, Carl-von-Linne-Weg, Cologne, 50829, Germany
3 - University of Cambridge, Department of Plant Sciences, Downing Street, Cambridge, CB2 EA3, UK

SUMMARY:
The expansion of plants onto land necessitated the evolution of robust defense strategies to protect against a wide array of microbial invaders. While host responses to microbial colonization are extensively explored in evolutionarily young land plant lineages like angiosperms, we know relatively little about plant-pathogen interactions in early diverging land plants thought to better represent the ancestral state. Here, we define the transcriptional and proteomic response of the early divergent liverwort *Marchantia polymorpha* to infection with the oomycete pathogen *Phytophthora palmivora.* We uncover a robust molecular response to oomycete colonization in *Marchantia* that consists of conserved land plant gene families. Direct macroevolutionary comparisons of host infection responses in *Marchantia* and the model angiosperm *Nicotiana benthamiana* further reveal a shared set of orthologous microbe-responsive genes that include members of the phenylpropanoid metabolic pathway. In addition, we identify a role for the *Marchantia* R2R3-MYB transcription factor MpMyb14 in activating phenylpropanoid (flavonoid) biosynthesis during oomycete infection. Mp*myb14* mutants infected with *P. palmivora* fail to activate phenylpropanoid biosynthesis gene expression and display enhanced disease susceptibility compared to wild-type plants. Conversely, the ectopic induction of Mp*Myb14* led to the accumulation of anthocyanin-like pigments and dramatically enhanced liverwort resistance to *P. palmivora* infection. Collectively, our results demonstrate that the *Marchantia* response to oomycete infection displays evolutionarily conserved features indicative of an ancestral pathogen deterrence strategy centered on phenylpropanoid-mediated biochemical defenses.

INTRODUCTION:

Plants have engaged in close-interactions with microbial life forms throughout their evolutionary history. Fossils obtained from the Rhynie chert demonstrate the presence of fungal hyphae and endosymbiotic structures within cells of >400 million-year old seedless vascular land plants, which suggests that the colonization and expansion of plants on land may be tightly linked with the ability to accommodate microbes [1,2]. Limited evidence also supports the idea that ancient land plants were attacked by pathogens, as oomycete-like organisms are present in fossilized plant detritus

in the Rhynie Chert [3,4]. Moreover, the fossils of *Nothia aphylla* (Early Devonian, vascular) cells colonized by fungus-like organisms display signatures of cell wall-associated responses that are typically directed to intruding filamentous microbes in extant plants [4,5]. The green plant lineage has since evolved and diversified into the various families present today, from the early diverging bryophytes (liverworts, mosses, and hornworts) to the evolutionarily young flowering seed plants (angiosperms). Our current understanding of how plants respond to microbes is heavily centered on angiosperms and is described in great detail at the metabolic, transcriptional, and proteome levels. In general, angiosperms employ a tiered immune system mediated by pattern recognition receptors (PRRs) that recognize broadly conserved microbial MAMPs (microbe-associated molecular patterns) or by nucleotide-binding leucine-rich repeat (NLR) proteins that directly/indirectly monitor pathogen virulence factors [6–8]. In many cases the activation of PRR or NLR-mediated immunity in angiosperms leads to the conserved induction of defense hormones (salicylic acid, jasmonic acid), secretion of pathogenesis-related (PR) proteins, cell-wall reinforcement, and phenylpropanoid-associated biochemical defenses (polyphenols, flavonoids, anthocyanins, phytoalexins) [8–10]. By comparison, we know relatively little about how early diverging land plant lineages respond to invading microbes, which limits our ability to identify core plant defense mechanisms representative of ancestral traits that likely contributed to the colonization and expansion of plants on land.

Bryophytes are non-vascular, gametophyte-dominant (haploid) land plants that are thought to have evolved key traits essential to life on land. Recent phylogenetic analyses suggest that the bryophytes represent a monophyletic group of early diverging land plants, wherein liverworts and mosses are united in the 'Setaphyta' clade that is distinct from hornworts [11–13]. Evolutionarily conserved traits associated with metabolism, abiotic stress-tolerance, and plant development are well described in bryophyte model systems such as the moss *Physcomitrella patens* or the liverwort *Marchantia polymorpha* [14,15], however our understanding of their ability to sense and respond to microbes is only now being investigated in more detail [16–18]. Much of this effort has centered on interactions with beneficial symbiotic microbes, such as fungi belonging to the Glomeromycotina (arbuscular mycorrhizal fungi) or Mucoromycotina (Endogone fungi). These works have revealed the wide-spread conservation of plant genes essential for symbiosis across land plants and their algal-predecessors [19] and have also uncovered the physiological and environmental benefits of dual and contrasting fungal associations that likely shaped plant life on land [20]. Bryophyte-pathogen interactions are comparatively less well-resolved. In mosses, several pathosystems have been established between necrotrophic filamentous pathogens and the model moss *Physcomitrella patens* [16]. Recent studies have also revealed the conservation of MAMP/PRR-mediated immune pathways involved in the perception of fungal chitin epitopes in mosses [21]. Interactions with biotrophic or hemi-biotrophic pathogens (*Colletotrichum*, *Phytophthora*) that manipulate living plant cells have been investigated in *Physcomitrella*, however specialized intracellular microbial infection structures (such as haustoria) are not observed in these plants [22,23].

The dioecious liverwort *M. polymorpha* has gained significant traction as an early divergent bryophyte model system for comparative evolutionary analyses of molecular plant-microbe interactions. *M. polymorpha* and other bryophytes utilize a conserved "jasmonic acid" signalling

module that functions through the JA precursor dinor-OPDA (12-oxophytodienoic acid) rather than JA itself, indicative ligand-receptor co-evolution in the JA/OPDA pathway across plants [24]. This fits well with phylogenetic analyses of core plant immunity genes that appear to be conserved in the *M. polymorpha* genome [15]. An ecological survey of wild *M. polymorpha* liverworts identified several genera of endophytic fungi with beneficial or detrimental impacts on liverwort growth *in vitro*, however a mechanistic understanding of these interactions remains to be clarified [25]. We recently established a robust pathosystem between the hemi-biotrophic oomycete pathogen *Phytophthora palmivora* and *M. polymorpha*. *P. palmivora* hyphae efficiently colonize the dorsal photosynthetic layer of several liverwort species and develop intracellular infection structures that invaginate living host cells (biotrophy) specifically in this tissue layer [26]. Similar to observations in angiosperms, cellular trafficking machinery (Rab GTPases and the membrane syntaxin Mp*SYP13B*) were directed to intracellular infection structures in *Marchantia* [26], which suggests that phylogenetically distant land plants employ equivalent defense responses that may have been conserved throughout their evolutionary history. Ultimately, *P. palmivora* shifts to a necrotrophic lifestyle where plant tissues are actively destroyed to release additional nutrition.

In this study, we performed RNA-sequencing and proteome analyses to reveal molecular responses occurring in *M. polymorpha* liverwort thalli during infection with *P. palmivora.* This identified evolutionarily conserved loci responsive to pathogen infection that included small secreted PR proteins, transcription factors, and vesicular trafficking machinery among other gene families. To gain further evolutionary insight, we performed comparative RNA-seq analysis against a *Phytophthora*-angiosperm (*Nicotiana benthamiana*) leaf infection time-course, which facilitated the discovery of orthologous groups of pathogen-responsive *Marchantia* and *Nicotiana* genes associated with phenylpropanoid/flavonoid biosynthesis. Consistent with these data, we uncovered a role for a phylogenetically basal R2R3 MYB transcription factor MpMyb14 in mediating flavonoid-associated biochemical defenses during pathogen infection in *M. polymorpha* thalli. Mp*myb14* mutants exhibited enhanced susceptibility to *P. palmivora* infection, whereas the ectopic over-accumulation of MpMyb14-regulated pigments dramatically suppressed pathogen growth *in planta*, suggesting a protective role for these compounds during biotic stress. Together these data provide further support for the conservation of biochemical defenses in phylogenetically distant model plants.

RESULTS

Dynamic alteration of the *Marchantia polymorpha* transcriptome and proteome during infection by *Phytophthora palmivora.*

To understand how *M. polymorpha* responds to infection, we performed time-resolved RNA-seq analysis comparing the transcriptional profiles of 3 week-old TAK1 (male) liverworts spot inoculated with water (mock) or a suspension of *P. palmivora* ARI-tdTomato (ARI-td) zoospores. Differential expression analysis (|LFC| >= 2 and adjusted p-value < 10^{-3}) of mock-vs-infected thalli sampled daily from 1-4 days post inoculation (dpi) revealed that infected liverworts undergo a pronounced shift in their transcriptional profiles compared to mock-treated controls, which is observed at 1 dpi and is strongest at 4 dpi (Figure 1AB, Data S1). The total number of differentially expressed genes gradually increased throughout the time course experiment to a maximum of 439 down-regulated and 968 up-regulated genes at 4 dpi (Figure 1B), with many of these genes

showing significant differential expression between 2-4 dpi (Figure 1C). To further support these data, we performed LC-MS/MS-based proteomics comparing *P. palmivora*-infected versus mock-treated TAK1 thalli at 4 and 8 dpi, which represent biotrophic and necrotrophic infection stages, respectively (Data S2). We identified 150 *M. polymorpha* proteins that were significantly enriched in *P. palmivora*-infected TAK1 thalli at both 4 and 8 dpi, with 93 proteins uniquely accumulating at 4 dpi during biotrophy and 262 proteins accumulating at 8 dpi during necrotrophy (Figure 1D, Data S2). A total of 137 proteins were consistently less abundant at both time points during infection, with only 76 proteins specifically depleted during biotrophy and 584 depleted proteins during the necrotrophic stage where plant tissues are actively destroyed by the pathogen (Figure 1D, Data S2). A comparison of the RNA-seq and proteomics datasets at 4 dpi (biotrophy) revealed 187 *M. polymorpha* loci that were consistently more abundant during infection and 36 loci that were consistently attenuated (Figure 1E). Together, these data reveal a dynamic molecular response in *M. polymorpha* thalli that are colonized by the hemibiotrophic oomycete *P. palmivora*.

Angiosperm Pathogenesis-Related (PR) gene families are similarly induced during infection in *Marchantia*

A hallmark of many plant-microbe interactions is the transcriptional induction of *pathogenesis-related* (*PR*) genes that typically encode small secreted proteins with predicted or demonstrated antimicrobial activity [27–29]. These families are generally conserved among seed plants and are expressed during various plant-microbe interactions [28,30]. To assess whether *PR* genes are similarly utilized in *M. polymorpha*, we identified candidate *PR* gene families (based on pfam domains) and assessed whether these loci are significantly upregulated in the *Marchantia-P. palmivora* RNA-seq infection time course. A number of candidate *PR* genes representing well-characterized families were identified (Figure S1), which encode small cysteine-rich secreted proteins (*PR1*), several glucanases and chitinases (*PR2, PR3, PR8, PR11*), protease inhibitors (*PR6*), subtilases (*PR7*), peroxidases (*PR9*), lipid transfer proteins (*PR14*), and cupins (*PR15/16*). Next, we increased the stringency of this search by identifying *PR* gene members displaying significant protein accumulation in the *Marchantia-Phytophthora* interaction proteome. This revealed support for the accumulation of PR1, PR2, PR3, PR5, PR6, PR9, and PR15 family members during infection (Figure 2A, Data S2). Notably, members of the *PR6* (protease inhibitor) and *PR9* (peroxidase) gene families were among the most highly induced loci observed in the *Marchantia-Phytophthora* time-course datasets and included the previously characterized Mp*PRX* (Mapoly0106s0049) locus [26]. To visualize the transcriptional induction of these loci *in planta*, we generated promoter-reporter lines in the TAK1 background and challenged thalli of these plants with *P. palmivora.* Transcriptional fusions of the Mp*PR6a* (Mapoly0448s0001) and Mp*PRX/PR9* promoters to nuclear-localized fluorescent reporters (tdTomato-NLS) demonstrated a strong induction of both genes during infection with YFP-labelled *P. palmivora* (isolate LILI) at 3 dpi (Figure 2B). The transcriptional induction of *MpPR6a* and *MpPRX/PR9* was observed in cells that were in direct contact with *P. palmivora* hyphae as well as uncolonized neighboring cells (Figure 2B). Analysis of *promoter:GUS* lines demonstrated that a 1.8-kb fragment of the Mp*PR6a* promoter was sufficient to drive GUS expression in *P. palmivora*-colonized air chambers along liverwort thalli compared to mock-treated controls (Figure 2C). This is in contrast to previously characterized Mp*PRX/PR9::GUS* lines that demonstrated a strong induction of GUS activity throughout the thallus of infected liverworts [26]. Collectively, these data demonstrate that PR

gene families are activated during the colonization of liverwort thalli by an oomycete pathogen in a manner similar to vascular plants, which suggests a conserved and perhaps ancestral role for PR gene families in plant-pathogen interactions across land plants.

Marchantia responds to pathogen infection with a diverse set of conserved gene families

To gain further insight into the classes of *M. polymorpha* loci responding to *P. palmivora* infection, we focused our analysis of the RNA-seq and proteomic datasets on the annotations and phylogenetic analyses of conserved land plant gene families described in [15]. This revealed a diverse set of *Marchantia* gene families responding to *P. palmivora* infection, including those associated with transcriptional regulation, the cell wall and cuticle, hormone biology, phenylpropanoid (flavonoid) biosynthesis, lipid peroxidation, terpene synthesis, vesicular trafficking, transporters/membrane H^+-ATPases, kinases and receptors (Figure 3A). Categorized heatmaps displaying the differential abundance of these loci during infection are displayed in Data S3. Using qRT-PCR analysis, we validated a subset of pathogen-responsive *Marchantia* loci, which showed significant increases in transcript abundance in TAK1 thalli infected with *P. palmivora* compared to mock-treated controls (Figure S2A). The RNA-seq analysis also confirmed the pathogen-induced upregulation of the membrane-localized syntaxin Mp*SYP13B* and dirigent-like Mp*DIR* genes that were previously demonstrated to be transcriptionally-induced during infection with *P. palmivora* [26]. Together, these data demonstrate the differential accumulation of broadly-conserved plant gene families during pathogen infection in *M. polymorpha* thalli.

A set of shared orthologous genes respond to oomycete colonization in *M. polymorpha* and the angiosperm *Nicotiana benthamiana*

Our expression studies in *Marchantia* suggested that liverworts activate conserved land plant gene families during infection with *P. palmivora.* However, the extent to which liverworts and angiosperms regulate the same groups of conserved orthologous genes during oomycete colonization was unknown. To address this, we performed infection time-course RNA-seq in the model angiosperm *Nicotiana benthamiana* for comparison against the *Marchantia-Phytophthora* transcriptome. Leaves of 3 week-old *N. benthamiana* plants were inoculated with *P. palmivora* ARI-td zoospores or water (mock-treatment) and analyzed at 14, 24, 48, and 72 hours post inoculation (hpi) since these time-points encompass comparable *P. palmivora* infection stages (early-to-late biotrophy and sporulation) [26,31]. RNA-seq analysis comparing mock-treated and *P. palmivora*-infected *N. benthamiana* leaves similarly revealed a prominent shift in transcriptional profiles during infection, with a steady increase in the total number differentially regulated genes at later stages of infection (Figure S2B). To compare the *Marchantia* and *Nicotiana* infection-expression profiles we first identified groups of orthologous protein-coding genes (orthogroups) using OrthoFinder [32]. This revealed a total of 7156 orthogroups shared between *M. polymorpha* and *N. benthamiana,* of which 2494 were single-copy orthologs likely representing genes with evolutionarily conserved functions. Since a large divergence time separates the evolution of liverworts and angiosperms, we assessed similarity in host responses to *Phytophthora* infection by focusing on the differential expression of single-copy orthologs shared in *M. polymorpha* and *N. benthamiana*. On average, ~80% of differentially expressed orthologs responded in the same direction across time-points (i.e. up- or down-regulated during infection in liverworts and angiosperms), while ~20% of loci responded in opposing directions (Figure 3B, Data S1). Several

of these responsive single-copy orthogroups belonged to conserved gene families, which included PR proteins, signalling machinery (MAPKs, RLKs, transcription factors), transporters, trafficking machinery, and cell wall-related proteins (Figure 3B). Genes classically associated with phenylpropanoid/flavonoid biosynthesis were among the most consistently/similarly responsive groups of conserved orthologous gene families activated during the colonization of liverwort and angiosperm host tissues by *P. palmivora* hyphae, with the exception of a single *C3'H* (*Coumarate 3'-hydroxylase*) gene that was downregulated in *Marchantia* and upregulated in *Nicotiana* (Figure 3BC). Collectively, these data reveal similarity in *Marchantia* and *Nicotiana* responses to pathogen infection despite the large phylogenetic distance separating liverworts and angiosperms.

P. palmivora infection activates Mp*Myb14* and a suite of flavonoid biosynthesis genes

In angiosperms, the biosynthesis of flavonoids and other polyphenolic compounds derived from phenylalanine/tyrosine (phenylpropanoids) are typically activated by developmental and stress-related programs via MYB transcription factors [33,34]. Our expression analysis of annotated *M. polymorpha* gene families showing conservation across land plants revealed a strong upregulation of the R2R3 MYB transcription factor Mp*Myb14* (Mapoly0073s0038) and several loci associated with flavonoid biosynthesis during infection of *Marchantia* thalli with *P. palmivora*. Previous reports have linked Mp*Myb14* expression with the biosynthesis of polyphenolic/flavonoid-like compounds that include the liverwort-specific anthocyanin Riccionidin A, which appears as a dark red/purple pigment in liverwort thalli during abiotic stress [35–37]. To confirm that Mp*Myb14* is induced during oomycete infection, we performed qRT-PCR analysis of mock- and *P. palmivora* ARI-td-treated TAK1 thalli over a 4 day infection time-course. A significant induction of Mp*Myb14* transcripts was observed from 2-4 dpi in *P. palmivora*-infected thalli relative to mock-treated controls (Figure 4A). Next, we compared our infection RNA-seq data (4 dpi timepoint) with that of Mp*Myb14*-overexpressing plants [37] to assess the extent to which MpMyb14 may influence the transcriptional response to pathogen infection in *Marchantia*. This comparison revealed 191 genes commonly activated during pathogen infection (19.7% of all pathogen-induced transcripts) and Mp*Myb14*-overexpression (Figure 4B), of which 20 were associated with flavonoid biosynthesis (Data S1). Such MpMyb14-regulated and infection induced genes included *chalcone synthases* (*CHS*), *phenylalanine ammonia lyases* (*PAL*), *chalcone-flavone isomerase-like* (*CHI-like*), and *cinnamate-4-hydroxylases* (*C4H*) among other enzymes. Using qRT-PCR analysis, we validated the upregulation of representative flavonoid biosynthesis genes (Mp*PAL,* Mp*CHS,* Mp*CHI-like*, and Mp*C4H*) in *P. palmivora*-infected TAK1 relative to mock-treated controls (Figure 4C). Together, these data suggest that *P. palmivora* infection activates the biosynthesis of flavonoids in *Marchantia* thalli. In support of this, we observed the accumulation of dark red/purple pigment in TAK1 thalli infected with *P. palmivora* ARI-td beginning from 4 dpi (Figure 4D). Characteristic anthocyanin-like pigment was most prominently observed around the walls of air chambers and epifluorescence microscopy revealed that *P. palmivora* ARI-td hyphae were largely absent in pigmented areas (Figure 4DF), which suggests that flavonoid biosynthesis may promote resistance to oomycete infection in *Marchantia.*

Marchantia Mp*myb14* mutants lack oomycete-induced phenylpropanoid biosynthesis gene induction and are highly susceptible to *P. palmivora*

To better ascertain the role of MpMyb14 during oomycete infection in *Marchantia*, we challenged Mp*myb14* knockout mutants [37] and a parental wild-type (TAK1) control with *P. palmivora.* Over a 7 day infection time-course, severe disease symptoms quickly developed in Mp*myb14* mutant lines (202f and 455r) compared to TAK1 (Figure 5A). To further support these observations, we performed qRT-PCR analysis of pathogen transcripts indicative of oomycete biomass (Pp*EF1a*) and sporulation (Pp*Cdc14*). Compared to the wild-type control, pathogen biomass and sporulation were significantly higher in both Mp*myb14* mutants (Figure 5B). Further analysis of MpMyb14-regulated phenylpropanoid/flavonoid biosynthesis gene expression [37] revealed significant reductions in pathogen-induced Mp*PAL*, Mp*CHS*, and Mp*CHI-like,* but not Mp*C4H,* in susceptible Mp*myb14* knockouts relative to the more resistant TAK1 control (Figure 5B). Collectively, these data identify a strong role for Mp*Myb14* in mediating liverwort resistance to oomycete infection.

The ectopic accumulation of MpMyb14-regulated pigment is associated with enhanced resistance to oomycete infection

The enhanced disease susceptibility of Mp*myb14* mutants and the diminished occurrence of *P. palmivora* hyphae in pigmented areas of TAK1 thalli suggested that flavonoid accumulation suppresses pathogen infection *in planta*. To investigate this further, we ectopically overexpressed Mp*Myb14* in TAK1 *M. polymorpha* liverworts and assessed the impact of anthocyanin overproduction on *P. palmivora* pathogenicity. Our initial efforts to establish constitutive $_{pro}$*35S:mCitrine*-Mp*Myb14* overexpression lines yielded highly pigmented plants with stunted growth (Figure S3A), which supports the idea that flavonoid overproduction negatively impacts liverwort growth [35]. To circumvent this issue, we generated heat shock-inducible Mp*Myb14* expression lines using the *HSP17.8A1* promoter [38,39]. In our conditions, this promoter demonstrated spurious activation in the absence of heat stress that resulted in a mosaic thallus displaying discrete sectors with pigment accumulation (Figure 6A). We took advantage of this phenotype and performed *P. palmivora* infection assays comparing colonization dynamics in pigmented sectors of $_{pro}$*HSP:*Mp*Myb14* plants relative to wild-type TAK1. Pigmented sectors inoculated with *P. palmivora* ARI-td zoospores remained relatively healthy over a 6 day infection time-course relative to non-pigmented sectors of the same plants or wild-type TAK1 controls (Figure 6AB). The preferential colonization of non-pigmented sectors of $_{pro}$*HSP:*Mp*Myb14* plants was further supported by epifluorescence microscopy, which revealed extensive hyphal growth and sporulation of red fluorescent *P. palmivora* in non-pigmented sectors relative to pigmented inoculation sites (Figure 6B). In support of these observations, qRT-PCR analysis revealed a significant reduction in pathogen biomass (Pp*EF1a*) and sporulation-associated (Pp*Cdc14*) transcripts in pigmented sectors of $_{pro}$*HSP:*Mp*Myb14* compared to wild-type TAK1 controls by 5 dpi (Figure 6C). To address whether Mp*Myb14*-overexpressing cells establish a hostile environment for invasive hyphae, we assessed whether pigmented sectors of $_{pro}$*HSP:*Mp*Myb14* liverworts display enhanced resistance to intracellular colonization compared to non-pigmented sectors or wild-type controls. Initial experiments using *P. palmivora* ARI-td suggested that intracellular infection structures were not established in pigmented sectors of $_{pro}$*HSP:*Mp*Myb14* relative to non-pigmented sectors and wild-type controls (Figure S3B). To further support this result, we generated a GFP-expressing *P. palmivora* strain (ARI-GFP*)* for compatible use with

propidium iodide staining to better discriminate between intra- and intercellular hyphal growth. In our experiments, propidium iodide fluorescence overlapped with phenylpropanoid metabolite autofluorescence in pigmented tissues (Figure S3C) but nevertheless discriminated between intra- and inter-cellular compartments. As expected, *P. palmivora* ARI-GFP was highly infectious and developed intracellular infection structures in TAK1 as well as non-pigmented $_{pro}$*HSP:*Mp*Myb14* sectors (Figure 6D). Similar to previous observations using *P. palmivora* ARI-td, intercellular hyphal growth was predominantly observed in pigmented sectors of $_{pro}$*HSP:*Mp*Myb14* (5/6 infection sites), however a single intracellular hyphal invasion event was observed in a single infection site (1/6) in only one of three experimental replicates (Figure 6D). Collectively, the data demonstrate that MpMyb14-regulated flavonoid/phenylpropanoid accumulation is associated with enhanced resistance to *P. palmivora* infection in *Marchantia*.

DISCUSSION:

In this study, we demonstrate that the early-divergent model liverwort *M. polymorpha* activates features of an evolutionarily conserved plant defense response during colonization by the pathogenic oomycete *P. palmivora.* This response was characterized by the induction of a number of gene families classically associated with defense, such as PR proteins, stress-associated enzymes, transcription factors, and cellular trafficking machinery. While several studies have demonstrated the upregulation of PR genes during angiosperm-pathogen interactions, limited evidence supports their conserved activation in distantly-related plant lineages. Transcriptomic and phylogenetic analyses identified conserved PR genes in gymnosperms (*Pinus tecunumanii* and *P. patula*) that were transcriptionally induced during interactions with the phytopathogenic fungus *Fusarium circinatum* [30]. Homologs of most PR families were represented in the genomes of selected gymnosperms and early diverging land plants (lycophytes, bryophytes), with exception of the PR12 (defensin) and PR13 (thionin) proteins that appear only in angiosperms [30]. Our analysis of *Marchantia PR* genes also failed to identify *PR12/PR13* homologs, which is consistent with the idea that these genes evolved later in the evolution of land plants. Additional studies have revealed the pathogen-induced expression of *PR1/PR10* homologs in the moss *P. patens* [40,41] and the differential regulation of *Azolla filiculloides* (water fern) *PR5/PR12* homologs in response to the defense hormone methyl-salicylate [42]. Together, these works suggest a conserved role for *PR* gene families in mediating responses to pathogens throughout the green plant lineage, with Mp*PR6a* (protease inhibitor) and Mp*PRX/PR9* (peroxidase) representing highly inducible members of the *M. polymorpha* PR complement. How these loci functionally contribute to this interaction is currently unknown, however expression profiles revealed by promoter-GUS fusions suggest that Mp*PR6a* (this work) may act in a more localized manner compared to Mp*PRX/PR9* [26]. It was previously suggested that the moss *Amblystegium serpens* employs a form of systemic acquired resistance (SAR) in response to localized MAMP treatments [43], however it remains to be seen if this response is observed during pathogen infection and whether functionally similar analogs of mobile angiosperm SAR signals are produced in early diverging lineages.

Adjustments in the *Marchantia* transcriptome caused by oomycete colonization include the differential regulation of transcription factor families conserved across land plants and in algal predecessors. The complement of pathogen-responsive transcription factors in *Marchantia* contained several families associated with responses to microbial colonization in angiosperms

(WRKY, GRAS, NAC, ERF, bHLH, MYB), which may hint at ancestral roles for these families in biotic and/or cellular stress tolerance. GRAS transcription factors are broadly implicated in the control of developmental programs and symbiotic plant-microbe interactions in angiosperms [44], with recent phylogenetic efforts demonstrating the conservation of key symbiosis-related GRAS clades in bryophytes [19,45]. Two *Marchantia* GRAS transcription factors were induced during infection with *P. palmivora*, which is consistent with previous work demonstrating the upregulation of the GRAS protein RAD1 during the colonization of *Medicago* roots by *P. palmivora* [46]. *Medicago rad1* mutants support similarly reduced levels of detrimental and beneficial microbes compared to wild-type controls, indicative of a regulatory role for RAD1 in controlling the intracellular colonization of plant tissues by microbes [46]. *M. polymorpha* does not support arbuscular mycorrhizal (AM) symbiosis and lacks a clear RAD1 ortholog, unlike other AM-competent liverworts [19,45]. Whether RAD1 and/or additional GRAS subfamilies (RAM, DELLA, etc) influence microbial colonization across land plants remains to be clarified and requires further phylogenetic and functional analyses, especially in AM symbiosis-supporting bryophytes like *Marchantia paleacea* or the hornwort *Anthoceros agrestis* [45,47]. WRKY transcription factors also represent a key gene family relevant to plant-pathogen interactions in angiosperms that is likely relevant across land plants [48,49]. Their importance in controlling plant immunity is further exemplified by the incorporation of WRKY domains as decoys coded within plant resistance proteins that monitor for interference of WRKY-mediated immune signalling caused by microbial effector proteins [50]. Such WRKY domain-containing R proteins are present in several monocot and dicot lineages [51], which suggests a prolonged and/or widespread evolutionary pressure to protect complex WRKY signalling pathways during the expansion of angiosperm lineages. A number of WRKY transcription factors were differentially expressed during colonization of *Marchantia* thalli by *P. palmivora*, which hints to a WRKY-mediated transcriptional response that fails to suppress oomycete colonization. Whether *P. palmivora* effectors manipulate conserved immune signalling modules (directly or indirectly) to promote microbial colonization in *Marchantia* and other land plants remains to be determined, but would begin to explain the success of this broad host-range pathogen in phylogenetically distant plant species.

To better understand the extent to which distantly related plants respond to microbial colonization, we compared the transcriptional response of *M. polymorpha* liverworts with that of the model angiosperm *N. benthamiana.* Remarkably, and despite millions of years of divergence time on a macroevolutionary timescale, we observed features of a common defense response activated by *P. palmivora* infection in both systems. This included several annotated categories of conserved plant genes involved in cell trafficking and signalling, and most strikingly included enzymes associated with the biosynthesis of phenylpropanoid/flavonoid-like metabolites. Phenylpropanoid-mediated biochemical defenses are commonly deployed during plant-pathogen interactions in angiosperms [52–54] and previous phylogenomic analyses have identified conserved phenylpropanoid metabolism genes in early diverging land plants [15,53]. We demonstrated that oomycete colonization induces phenylpropanoid metabolism in *Marchantia* thalli, which included the upregulation of enzymes associated with flavonoid biosynthesis such as phenylalanine ammonia lyase (PAL), chalcone synthase (CHS), chalcone-flavone isomerase-like (CHI-like), and cinnamate-4-hydroxylases (C4H). Importantly, these genes are similarly induced in oomycete-colonized angiosperms like *N. benthamiana* and in moss treated with microbial elicitors [21,55] or

infected with *Pythium irregulare* [40]. Together these data suggest that land plants have a shared capacity to launch phenylpropanoid-mediated biochemical defenses during infection.

The full complement of defense-related phenylpropanoid metabolites deployed in early divergent land plants is currently unknown, however we observed a clear accumulation of red/purple anthocyanidin pigment in oomycete-colonized thalli. Infection-induced pigment accumulation was concomitant with the upregulation of the MYB transcription factor MpMyb14 and a suite of flavonoid biosynthesis genes that were previously identified as MpMyb14-targeted loci important for flavonoid and anthocyanidin (Riccionidin A) biosynthesis [35,37]. This suggests that the pathogen-induced upregulation of phenylpropanoid metabolites like Riccionidin A are routed through MpMyb14 in *Marchantia*, which was supported by the ~20% overlap in the transcriptional profiles of oomycete-infected thalli and Mp*Myb14*-overexpressing plants. Previous studies have demonstrated a role for MpMyb14 in activating anthocyanidin accumulation in response to abiotic stressors such as nutrient deprivation, light stress, high NaCl, and exposure to UV-B [35–37]. These studies further demonstrated a protective function for MpMyb14-regulated flavonoids against oxidative stress [37], which provided flavonoid hyper-accumulating Mp*Myb14*-overexpression lines with enhanced tolerance to UV-B exposure [36]. Here, we show that Mp*myb14* mutants lack oomycete-induced flavonoid/phenylpropanoid biosynthesis gene induction and are more susceptible to *P. palmivora* infection, which suggests a role for flavonoid biosynthesis in liverwort disease resistance. Consistent with this idea, we observed that MpMyb14-associated pigment accumulation provides *Marchantia* thalli with enhanced resistance to *P. palmivora* infection. Pigmented areas of wild-type plants displayed reduced levels of pathogen hyphae and pigmented sectors of Mp*Myb14*-overexpressing thalli supported reduced levels of pathogen growth relative to non-pigmented sectors and wild-type controls. Given that MpMyb14-associated phenylpropanoid metabolites afford thalli with enhanced tolerance to oxidative stress, it is likely that this function is at least partly responsible for the bolstered resistance to *P. palmivora* infection. However, we cannot rule out the possibility that the complement of MpMyb14-regulated metabolites includes an antimicrobial or cell wall-strengthening compound that is highly effective against *P. palmivora*. Indeed, pigmented sectors of $_{pro}$*HSP:*Mp*Myb14* liverworts exhibited fewer events of intracellular colonization, which may suggest a role for Riccionidin A in cell wall-associated defenses. Since MpMyb14 regulates both early and late steps of the phenylpropanoid pathway, specific Riccionidin A biosynthesis mutants are required to understand its role in defense. In angiosperms, a diverse set of phenylpropanoid metabolites (colorless flavonoids, anthocyanin pigments, cinnamic acids, lignins/lignans, etc) have demonstrated antimicrobial, antioxidative, and cell wall reinforcement activities that contribute to plant resistance against microbial infection [53,54,56–58]. While early divergent land plants belonging to the bryophytes lack lignin, it was recently suggested that the phenol-enriched cuticle and cell wall of the moss *P. patens* may represent an ancestral feature critical to the expansion of plants onto land [59]. Whether pathogen-induced phenylpropanoids contribute to modifications of phenolic *Marchantia* cell walls during infection remains a possibility, as Riccionidin A pigment is predominantly integrated into liverwort cell walls [35,37] whereas colorless flavonoids similarly regulated by MpMyb14 remain in the cytosol [37]. A suite of dirigent (*DIR*) genes, which have been associated with lignin/lignan biochemistry in angiosperms [60], are upregulated alongside phenylpropanoid biosynthesis genes during oomycete infection and may

contribute to chemical complexity in phenolic cell walls of bryophytes. Collectively, these observations suggest that MpMyb14 regulates a suite of phenylpropanoid metabolites that fulfil multiple roles in protecting liverwort thalli from biotic and abiotic stress.

Flavonoid biosynthesis is generally controlled by the MBW (R2R3-MYB, bHLH, WD40) protein complex in angiosperms [33,34]. In early diverging plant lineages like liverworts it is not yet clear whether such a complex exists, but evidence supports the role of certain R2R3-MYB and bHLH transcription factors in regulating flavonoid biosynthesis [35,37,61]. Phylogenetic analysis places the *Marchantia* MpMyb14 protein basal to the MYB subgroups SG4-SG7, which generally represent key activators and repressors (SG4) of flavonoid biosynthesis in angiosperms [35]. Since MpMyb14 is a transcriptional activator, it is possible that the ancestral role of this R2R3-MYB lineage was to activate flavonoid biosynthesis, perhaps independent of a conserved MBW complex since MpMyb14 lacks bHLH-interacting domains [35]. While the majority of angiosperms lack the capacity to synthesize Riccionidin A specifically, several R2R3-MYBs have been shown to control a diverse array of flavonoids/anthocyanins during development and stress [33,34,54]. In Arabidopsis, the SG6 MYB PAP1/MYB75 positively regulates anthocyanin accumulation in response to several environmental stimuli [62–65]. PAP1-mediated anthocyanin accumulation has also been linked to the JA signalling pathway, wherein JAZ-mediated repression of PAP1 is lifted upon JA accumulation, leading to pigment accumulation during stress [66]. Since *Marchantia* encodes a conserved COI1-JAZ module responsive to the JA precursor dn-OPDA [24], it is possible that this pathway similarly regulates flavonoid biosynthesis during biotic stress in liverworts. In any case, our study and others demonstrate that the complex regulation of flavonoid biosynthesis by MYB and bHLH transcription factors has deep evolutionary roots, with functions in stress tolerance that are present even in early divergent land plants [35–37,61]. The charophytic algal predecessors of land plants encode phenylpropanoid biosynthesis genes and have a capacity for embryophyte-like stress signalling [67,68] yet lack orthologs of Mp*Myb14* and other flavonoid-regulating R2R3-MYB transcription factors [15,37]. It therefore appears that the evolution of R2R3-MYB-mediated control of an expanding flavonoid/phenylpropanoid metabolite repertoire likely facilitated key advances in plant development (vertical growth) and stress physiology (antimicrobials, sunscreens, antioxidants, etc) that were essential for the expansion of plant life on land [15,35,37,69].

Evolutionary plant-pathogen interaction studies have typically focused on tightly co-evolving relationships within plant and microbial populations [70]. Here, we took a comparative macroevolutionary approach that identified conserved orthologous plant genes responsive to oomycete infection in early and late diverging land plant lineages. This analysis uncovered a set of pathogen-responsive orthologous genes with roles in vesicular trafficking, antimicrobial defenses, transcriptional control, cell signalling, and stress-associated metabolism. Using this knowledge, we identified a conserved role for phenylpropanoid-associated biochemical defenses in mitigating pathogen infection in liverworts, which presents as an ancestral layer of the plant basal defense response that was likely critical for the expansion of plants on land. Collectively, this work provides key evolutionary insight into the nature of early land plant defense strategies that are shared with distantly-related lineages. Future studies on host responses to oomycete

infection across diverse land plant lineages (lycopods, ferns, gymnosperms) are likely to reveal additional layers of plant immunity that evolved to protect derived land plant features.

ACKNOWLEDGEMENTS

We thank Anne Harzen for support with proteomics efforts, Edwige Moyroud (Sainsbury Laboratory, Cambridge) for commenting on an earlier draft of the manuscript, and Edouard Evangelisti for advice on *Phytophthora* transformation. For additional critical and technical support, we thank Natalia Guayazan Palacios and all members of the Schornack group. This work was funded by the Gatsby Charitable Foundation (GAT3395/GLD), the Royal Society (UF160413, RGF\EA\180002), the BBSRC OpenPlant initiative (BB/L014130/1), the Natural Environment Research Council (NERC; NE/N00941X/1), and a Natural Sciences and Engineering Research Council of Canada (NSERC) postdoctoral fellowship to PC. Proteomic work performed in the Nakagami lab was supported by the Max-Planck-Gesellschaft.

AUTHOR CONTRIBUTIONS

PC, AG, and SS designed research; PC, AG, DJH, AJB, and SCS performed the research; PC, AG, SCS, HN and SS analyzed data; SCS and HN performed proteomic analysis; PC and SS wrote the paper with technical contributions from AG and SCS.

DECLARATION OF INTERESTS

The authors declare no competing interests.

FIGURE LEGENDS

Figure 1. *Marchantia polymorpha* undergoes a dynamic transcriptional and proteomic response during infection with *Phytopthora palmivora*

(A) Hierarchical clustering of significantly differentially expressed genes during *P. palmivora* infection (adjusted p-value < 10^{-3}, log fold change (|LFC| $\geqslant$ 2), variance-stabilised row-centered counts are shown. Time points represent days post infection (dpi).

(B) Volcano plots displaying pairwise differential expression analysis per time point of *P. palmivora*-infected versus mock-treated samples at the indicated time points. Significantly differentially expressed genes are displayed in red.

(C) Upset plots showing shared and time point-specific up-regulated and down-regulated *M. polymorpha* genes.

(D) Total numbers of differentially abundant (enriched or depleted) *M. polymorpha* protein groups in *P. palmivora*-infected versus mock-treated liverworts at 4 and 8 dpi.

(E) Comparison of differentially regulated *M. polymorpha* loci identified at 4 dpi in the RNA-seq and proteomics analyses. See also Data S1-S2.

Figure 2. Pathogenesis-related (PR) protein families are activated in oomycete-colonized *M. polymorpha* thalli

(A) Identification and description of *M. polymorpha PR* gene families displaying transcript and protein accumulation during infection with *P. palmivora*. See also Data S1-S2 and Figure S1.

(B) Visualization of Mp*PR6a* and Mp*PRX/PR9* promoter activation in air chambers of 3-week-old $_{pro}$Mp*PR6a:tdTomato-NLS* and $_{pro}$Mp*PRX/PR9:tdTomato-NLS* lines 3 days post infection with *P. palmivora*-YFP (isolate LILI-KDEL-YFP) or mock-treated with water. Air pores (AP) are labelled at the centre of the pore. Scale bars = 50 µm.
(C) Tissue level expression analysis of $_{pro}$Mp*PR6a:GUS* liverworts infected with *P. palmivora* (ARI-td) or mock-treated with water. Cross sectioned thalli were stained 7 days post infection. An arrow indicates an air pore (AP) on the dorsal liverwort surface. Scale bar = 0.5 mm. All images are representative of results collected from at least 6 independent treatment (mock or infected) sites.

Figure 3. Oomycete-colonized *M. polymorpha* liverworts exhibit features of an evolutionarily conserved transcriptional response to pathogen infection
(A) Alluvial diagrams summarizing overall transcriptional dynamics of *M. polymorpha* gene families that are differentially expressed during infection. Relative width of the alluvial band corresponds to the number of differentially expressed genes at a given time point (Abbreviations: dpi - days post inoculation; MAPK - map kinase; PR - pathogenesis-related; TF - transcription factor; RLK - receptor-like kinase).
(B) Similarity of transcriptional responses of single-copy orthologous genes in *P. palmivora* (ARI-td)-infected *M. polymorpha* thalli and *N. benthamiana* leaves. Scatter plots display the direction (LFC = log2 fold change) of transcriptional changes of single-copy orthologs during infection in both hosts. Significantly differentially expressed single copy orthologs with adjusted p-value < 10^{-3} are shown.
(C) Differential expression of single-copy phenylpropanoid pathway-related genes in *M. polymorpha* and *N. benthamiana* during oomycete infection. Variance-stabilised row-centered counts are shown for *P. palmivora* infected plant samples. See also Data S1, Data S3 and Figure S2.

Figure 4. Mp*Myb14* upregulation coincides with the induction of flavonoid biosynthesis genes and pigment accumulation in *P. palmivora*-colonized *Marchantia* thalli
(A) qRT-PCR analysis of Mp*Myb14* transcripts in mock-treated or *P. palmivora*-colonized (ARI-td) TAK1 plants (n = 8 per timepoint/treatment) from 1 to 4 days post inoculation (dpi). Expression values are shown relative to internal Mp*ACT* and Mp*EF1a* controls. Different letters signify statistically significant differences in transcript abundance (ANOVA, Tukey's HSD, P < 0.05).
(B) Overlap between transcriptional profiles of Mp*Myb14*-overexpressing (OX) liverworts [37] compared to *P. palmivora*-infected TAK1 thalli at 4 dpi. See also Data S1.
(C) qRT-PCR analysis of phenylpropanoid/flavonoid pathway genes (Mp*PAL - Phenylalanine Ammonia Lyase* Mapoly0005s0089*;* Mp*CHS - Chalcone Synthase* Mapoly0021s0159*;* Mp*CHI-like - Chalcone-flavone Isomerase-like* Mapoly0175s0004*;* Mp*C4H - Cinnamate-4-Hydroxylase* Mapoly0163s0018) in mock-treated or *P. palmivora*-colonized (ARI-td) TAK1 plants from 1 to 4 dpi. Expression values are shown relative to internal Mp*ACT* and Mp*EF1a* controls. Different letters signify statistically significant differences in transcript abundance (ANOVA, Tukey's HSD, p < 0.05).
(D) Bright-field micrographs of mock-treated (water) and *P. palmivora*-infected TAK1 thalli (5 dpi) illustrating pathogen-dependent accumulation of anthocyanin-like pigment (purple) around air chambers on the dorsal thallus surface. Scale bars = 1 mm (n = 8).

(E) Bright-field and epifluorescence micrographs illustrating the lack of *P. palmivora* ARI-td (red fluorescent) hyphae in pigmented (arrows) areas of TAK1 liverwort thalli at 5 dpi (n = 8).

Figure 5. Mp*Myb14*-dependent regulation of flavonoid biosynthesis genes is required for liverwort resistance to oomycete infection

(A) Macroscopic phenotypes of 3-week-old Mp*myb14* mutant (202f and 455r) and wild-type (TAK1) liverworts 5 days post inoculation (dpi) with *P. palmivora* ARI-td. Scale bar = 1 cm (n = 5).
(B) Quantification of *P. palmivora* biomass (Pp*EF1a*), sporulation (Pp*Cdc14*) and phenylpropanoid biosynthesis genes (Mp*C4H*, Mapoly0163s0018; Mp*PAL*, Mapoly0005s0089; Mp*CHS*, Mapoly0021s0159; Mp*CHI-like*, Mapoly0175s0004) during *P. palmivora* ARI-td-infection in wild-type (TAK1) and Mp*myb14* (202f and 455r) mutant liverworts *at* 1, 3, and 5 dpi (n = 8 per treatment/timepoint). Gene expression was quantified relative to the *M. polymorpha* biomass markers Mp*ACT* and Mp*EF1a*. Different letters signify statistically significant differences in transcript abundance (ANOVA, Tukey's HSD, $p < 0.05$).

Figure 6. The ectopic over-accumulation of MpMyb14-regulated phenylpropanoids enhance resistance to *P. palmivora*

(A) Macroscopic phenotypes of 3-week-old $_{pro}$*HSP:*Mp*Myb14* and wild-type (TAK1) liverworts 7 days post inoculation (dpi) with *P. palmivora* ARI-td. Scale bar = 1 cm (n = 8).
(B) Bright-field and epifluorescence micrographs demonstrating the differential colonization of $_{pro}$*HSP:*Mp*Myb14* thalli by *P. palmivora* ARI-td (red fluorescence) at 5 dpi. Pigmented sectors appear dark purple whereas non-pigmented sectors are green. An arrow indicates the site of *P. palmivora* zoospore inoculation in a pigmented sector. Scale bar = 0.1 cm (n = 8).
(C) Quantification of *P. palmivora* biomass (Pp*EF1a*) and sporulation (Pp*Cdc14*) marker genes during the colonization of pigmented sectors of $_{pro}$*HSP:*Mp*Myb14* compared to wild-type (TAK1) plants at 1, 3, and 5 dpi (n = 8 plants per timepoint/treatment). *Phytophthora* marker gene expression was quantified relative to the *M. polymorpha* biomass markers Mp*ACT* and Mp*EF1a*. Different letters signify statistically significant differences in transcript abundance (ANOVA, Tukey's HSD, $p < 0.05$).
(D) Confocal fluorescence microscopy demonstrating intracellular colonization phenotypes of TAK1 and green (non-pigmented) versus purple (highly pigmented) sectors of $_{pro}$*HSP:*Mp*MYB14* liverworts infected with *P. palmivora* GFP (3 dpi). Pathogen fluorescence (GFP) is overlaid with propidium iodide staining (red) to discern intra- versus intercellular hyphal growth *in planta*. Branched or digit-type haustoria are denoted with an asterisk while invasive hyphae are indicated by an arrow. Occurrence of the observed structures in (n = 6) infected liverworts is denoted per representative image. See also Figure S3.

STAR Methods Text

CONTACT FOR REAGENT AND RESOURCE SHARING

"Further information and requests for resources and reagents should be directed to and will be fulfilled by the Lead Contact, Sebastian Schornack (sebastian.schornack@slcu.cam.ac.uk)."

EXPERIMENTAL MODEL AND SUBJECT DETAILS

Plant Growth Details

Marchantia polymorpha TAK1 (male) liverworts were cultivated from gemmae under axenic conditions on one-half–strength MS (Murashige and Skoog) media (pH 6.7) supplemented with B5 vitamins under continuous light (70 µE·m−2·s−1) at 22 °C. *Nicotiana benthamiana* plants were grown on soil in glasshouse conditions with a controlled temperature of 22-24 °C and long-day photoperiod (16 hours of light).

Pathogen Growth Details

The fluorescently labelled *Phytophthora palmivora* strains ARI-td (accession P3914; [71]), ARI-GFP (this study), and LILI-YKDEL (accession P16830; [31]) used in this study were grown in a Conviron growth cabinet set to 25 °C with constant light conditions that are maintained routinely by passaging zoospores onto V8 juice agar plates supplemented with G418 (100 µg/mL) and carbenicillin (50 µg/mL).

METHOD DETAILS

Pathogen Infection Assays

Pathogen colonization experiments were performed by applying 10-µL droplets of a zoospore suspension inoculum (10^5 zoospores per milliliter) along the dorsal thallus surface of 3-week-old *M. polymorpha* liverworts or onto the abaxial surface of detached *N. benthamiana* leaves collected from 3-week-old plants that were subsequently kept on wetted absorbent paper enclosed in plastic dishes to maintain high humidity.

Phytophthora palmivora Transformation

Transformation of *P. palmivora* ARI (accession P3914) with pTOR-GFP [72] was performed as described in [73]. In brief, approximately 40 µg of pTOR-GFP vector was added to 680 µL of a concentrated suspension of ARI zoospores and 80 µL of 10X Petri's solution (2.5 mM $CaCl_2$, 10 mM $MgSO_4$, 10 mM KH_2PO_4, 8 mM KCl). This suspension was electroporated with the following settings: voltage at 500 V, capacitance at 50 F, resistance at 800 ohms, with a time constant around 6-7 ms. The electroporated suspension was combined with 6 mL of clarified liquid V8 media in a 15 mL falcon tube and incubated on a gentle rocking shaker for 6 hours at room temperature. Positive GFP expressing transformants were selected on V8 plates containing G418 (100 µg/mL) and carbenicillin (50 µg/mL) 3-10 days after plating.

Microscopy & Histochemical Staining

Confocal laser scanning microscopy was performed using a Leica TCS SP8 equipped with HyD detectors as described in [26]. A white light laser was used to visualize GFP (excitation 488 nm), mCitrine (excitation 509 nm) and YFP (excitation 515 nm). Epifluorescence microscopy was performed on a dissecting Leica M165 FC stereo-epifluorescence microscope using a DSRed filter for the detection of tdTomato fluorescence. Images were obtained using Leica Application

Suite V4.1 acquisition software. Images were collected from at least three independent plants in at least two separate infection sites per plant. All experiments were performed at least three times with similar results. Histochemical GUS staining was performed on ARI-td-infected liverworts by vacuum infiltrating plants with a GUS staining solution consisting of 2 mM X-gluc (5-bromo-4-chloro-3-indolyl-beta-D-glucuronic acid, cyclohexylammonium salt), 0.1 % Triton X-100, 10 mM EDTA, 2.5 mM potassium hexacyanoferrate II, and 2.5 mM potassium hexacyanoferrate III in a buffered phosphate solution (3.1 g/L sodium phosphate monobasic monohydrate and 10.9 g/L sodium phosphate dibasic anhydrous in double distilled water, pH 7.4). Plants were incubated in staining solution overnight (12-16 hours) at 37 °C and were subsequently de-stained in a solution of 70% ethanol with 20% glycerol added. Cross-sections of GUS-stained liverworts were prepared at a thickness of 200-to-300-µm from 3% agarose-embedded samples using a vibratome. All images were processed using ImageJ or Microsoft Powerpoint. Propidium iodide (PI) staining was performed by incubating excised liverwort thalli in 2 µg ml^{-1} propidium iodide solution (in water) for 15 minutes in the dark. PI fluorescence was visualized by confocal laser scanning microscopy (excitation 543 nm, emission detected at 588-628 nm). For analysis of heavily pigmented sectors, on those areas of $_{pro}$*HSP:*Mp*Myb14* where no light transmittance is observable in the bright field channel was considered.

RNA Isolation, cDNA Synthesis, and qRT-PCR Analysis

Total RNA was extracted from flash-frozen *M. polymorpha* (TAK1) plants that were mock-inoculated (water) or infected with *P. palmivora* (ARI-td) zoospores using the PureLink Plant RNA Reagent following the manufacturer's instructions. All total RNA samples were subsequently treated with Turbo DNA-free DNAse reagent (Invitrogen) to degrade residual DNA contamination before further use. cDNA was synthesized with SuperScript II reverse transcriptase (Invitrogen) using 2 µg of total RNA following the manufacturer's instructions. All cDNA samples were diluted 10-fold with nuclease-free water and stored at −20 °C. qRT-PCR analyses were carried out in 10 µL reactions using 2.5 µL of diluted cDNA and Roche SYBR mix with the primers listed in Table S1. All qRT-PCR experiments were performed using a program consisting of an initial denaturation at 95 °C for 5 minutes followed by 40 cycles of 95 °C for 10 seconds, 60 °C for 14 seconds, and 72 °C 14 seconds on a Roche LightCycler 480 II according to manufacturer's instructions. Primers for qRT-PCR analyses were designed using Primer3 [74,75] and specificity was validated by analyzing melt curves after each run. This study also used previously published primers for *M. polymorpha* housekeeping genes [76], *P. palmivora* transcript quantification [71], and *M. polymorpha* phenylpropanoid pathway analysis [37] (Table S1). Three technical replicates were analyzed for each of three independent sample replicates at any given time point/treatment. Calculations of expression levels normalized to internal controls and statistical analyses (ANOVA, Tukey's HSD) were performed using R software. Graphs were generated in GraphPad Prism6.

Proteomics

Sample preparation: 50 mg of powdered *M. polymorpha* tissue were added to 250 µL of extraction buffer (8M Urea in 100mM Tris/HCl pH8.5, complemented with Phosphatase Inhibitor Cocktail 3 (Sigma, P0044-5ML) (20 µl/ml) and Phosphatase Inhibitor Cocktail 2 (Sigma, P5726-5ML) (20 µl/ml) and briefly mixed on a Vibrax shaker. Next, all samples were sonicated for 15 min and subsequently mixed on a Vibrax shaker for 15 min. After determination of the protein concentration using Pierce 660nm Protein Assay, aliquots of 100 µg total protein per sample were further processed by in-solution digest. Protein mixtures were reduced with dithiothreitol, alkylated

with chloroacetamide, and digested first with Lys-C for 4h and subsequently with trypsin overnight. Samples were then submitted to SDB-RPS fractionation using a protocol adapted from [77]. In brief, stage tips were prepared with 2 layers of SDB-RPS membrane and activated with 100 µL acetonitrile, followed by equilibration with 100 µL equilibration buffer (30% (v/v) MeOH, 1% (v/v) TFA) and 100 µL 0.2% TFA. Peptides were immobilized on the membrane, washed with 100 µL 0.2% TFA, eluted into 3 consecutive fractions using SDB-RPS buffer 1 (100 mM NH4HCO2, 40% (v/v) ACN, 0.5% FA), SDB-RPS buffer 2 (150 mM NH4HCO2, 60% (v/v) ACN, 0.5% FA) and finally SDB-RPS buffer 3 (5% Ammonia (v/v), 80% (v/v) ACN). The collected fractions were evaporated to dryness to remove residual ammonia.

LC-MS/MS data acquisition: dried peptides were re-dissolved in 2% ACN, 0.1% TFA for analysis and adjusted to a final concentration of 0.1 µg/µl. Samples were analysed using an EASY-nLC 1200 (Thermo Fisher) coupled to a Q Exactive Plus mass spectrometer (Thermo Fisher). Peptides were separated on 16 cm frit-less silica emitters (New Objective, 0.75 µm inner diameter), packed in-house with reversed-phase ReproSil-Pur C18 AQ 1.9 µm resin. Peptides (0.5 µg) were loaded on the column and eluted for 115 min using a segmented linear gradient of 5% to 95% solvent B (0 min : 5%B; 0-5 min -> 5%B; 5-65 min -> 20%B; 65-90 min ->35%B; 90-100 min -> 55%; 100-105 min ->95%, 105-115 min ->95%) (solvent A 0% ACN, 0.1% FA; solvent B 80% ACN, 0.1%FA) at a flow rate of 300 nL/min. Mass spectra were acquired in data-dependent acquisition mode with a TOP15 method. MS spectra were acquired in the Orbitrap analyzer with a mass range of 300–1750 m/z at a resolution of 70,000 FWHM and a target value of 3×106 ions. Precursors were selected with an isolation window of 1.3 m/z. HCD fragmentation was performed at a normalized collision energy of 25. MS/MS spectra were acquired with a target value of 105 ions at a resolution of 17,500 FWHM, a maximum injection time of 55 ms and a fixed first mass of m/z 100. Peptides with a charge of +1, greater than 6, or with unassigned charge state were excluded from fragmentation for MS2, dynamic exclusion for 30s prevented repeated selection of precursors.

Data analysis. Raw data were processed using MaxQuant software (version 1.5.7.4, http://www.maxquant.org/) [78] with label-free quantification (LFQ) and iBAQ enabled [79]. MS/MS spectra were searched by the Andromeda search engine against a combined database containing the sequences from *M. polymorpha* (primary transcripts; http://marchantia.info/download/download/Mpolymorphav3.1.primaryTrs.pep_annot.fa.gz), *Phytophthora palmivora* [80] and sequences of 248 common contaminant proteins and decoy sequences. Trypsin specificity was required and a maximum of two missed cleavages allowed. Minimal peptide length was set to seven amino acids. Carbamidomethylation of cysteine residues was set as fixed, oxidation of methionine and protein N-terminal acetylation as variable modifications. Peptide-spectrum-matches and proteins were retained if they were below a false discovery rate of 1%. Statistical analysis of the MaxLFQ values was carried out using Perseus (version 1.5.8.5, http://www.maxquant.org/). Quantified proteins were filtered for reverse hits and hits “identified by site” and MaxLFQ values were log2 transformed. After grouping samples by condition (4 groups) only those proteins were retained for the subsequent analysis that had two valid values in one of the conditions. Missing values were imputed from a normal distribution, using the default settings in Perseus (1.8 downshift, separately for each column). Volcano plots were generated in Perseus using an FDR of 0.01 and an s0=1, data was exported and processed

using Excel. For comparisons against RNA-seq data, we considered significantly differentially abundant protein loci (LFC > 1) with 1 unique peptide fragment identified in the fractionated analyses that mapped to the *Marchantia polymorpha* proteome.

Cloning and *Marchantia* Transformation

Promoter regions of Mp*PR6a* (Mapoly0448s0001) and Mp*PRX/PR9* (Mapoly0106s0049; described in [26] and the coding region of Mp*Myb14* (Mapoly0073s0038) were synthesized with flanking attL sites by Genewiz for direct recombination into *Marchantia* Gateway destination vectors [39]. The $_{pro}$Mp*PR6a*/Mp*PRX*:*tdTomato-NLS* and $_{pro}$Mp*PR6a:GUS* constructs were generated by recombination into pMpGWB316 and pMpGWB104 using LR clonase II enzyme mix (invitrogen) according to the manufacturer's directions. MpMyb14 expression vectors were similarly generated by LR recombination into pMpGWB105 ($_{pro}$*35S:mCitrine-flag*-Mp*Myb14*) and pMpGW132 ($_{pro}$*HSP:flag*-Mp*Myb14*). The resulting constructs were transformed into *Agrobacterium tumefaciens* GV3101 (pMP90) by electroporation. *M. polymorpha* transformation was carried out using the *Agrobacterium*-mediated thallus regeneration method using TAK1 plants [81]. Transformants were selected on solidified 1/2 MS media (pH 5.6) supplemented with cefotaxime (125 µg/mL) and hygromycin B (15 to 25 µg/mL) or chlorsulfuron (0.5-1 µM). Stable, non-chimeric transgenic plants were obtained by propagating gemmae from T1 thalli.

Library preparation and sequencing

mRNAs from *M. polymorpha* plants infected with *P. palmivora* ARI-td at 1, 2, 3 and 4 dpi, and *N. benthamiana* leaves infected with *P. palmivora* ARI-td at 14, 24, 48 and 72 hpi and respective mock-inoculated control samples were purified using Poly(A) selection from total RNA sample, and then fragmented (at least 2 independently infected plants collected per sample replicate). cDNA library preparation was performed with the TruSeq® RNA Sample Preparation Kit (Illumina, US) according to the manufacturer's protocol. cDNA sequencing of each sample (all in triplicates) was performed with Illumina HiSeq 2500 in 100 (*Marchantia*) or 150 (*Nicotiana*) paired end mode. Samples were de-multiplexed and analyzed further. The raw fastq data are accessible at http://www.ncbi.nlm.nih.gov/sra/ with accession numbers PRJNA397637 (*Marchantia-Phytophthora*) and PRJNA503573 (*Nicotiana-Phytophthora*).

Expression analysis

Raw reads first analysed with FastQC for quality control (https://www.bioinformatics.babraham.ac.uk/projects/fastqc/) were aligned back to the respective plant genome (Marchantia polymorpha v3.1 and *Nicotiana benthamiana* draft genome sequence v1.0.1) using STAR (version 2.5.2b) aligner [82]. Raw counts were obtained with featureCounts [83] and only uniquely mapped and properly paired reads were considered further. Differentially expressed genes were identified with DESeq2 Bioconductor package [84] following pair-wise comparisons between infected and mock-inoculated samples at the same stage of infection. Differentially expressed genes (absolute LFC [log2 fold change] ≥ 2 and adjusted p-value ≤ 10^{-3}) were used to perform hierarchical clustering of samples. Heatmaps for the differentially expressed genes were generated using R pheatmap package using variance-stabilised counts median-centered by gene. Scripts used to analyse RNA-seq datasets and visualise differentially expressed genes are available at https://github.com/gogleva/Marchantia. Summary *M.*

polymorpha functional gene annotations were created based on [15]. Tidy summary annotations are also available at https://github.com/gogleva/Marchantia. Alluvial diagrams displaying the dynamics of annotated *M. polymorpha* genes differentially expressed during *P. palmivora* infection were performed in R using the 'alluvial' package.

Orthology analysis

To reconstruct orthogroups between *M. polymorpha* and *N. benthamiana*, we used OrthoFinder (OrthoFinder-2.2.7; [32]) with respective plant proteomes. For this analysis only primary protein isoforms were used. Output files were parsed and further analysed in R (scripts and raw outputs are available at https://github.com/gogleva/Marchantia). Following differential expression analysis (only genes with adjusted p-value < 10^{-3} were considered), we used LFC of single-copy orthologs to assess similarity of *M. polymorpha* and *N. benthamiana* responses to infection with *P. palmivora* (strain ARI-tdTomato). Based on previous characterization of *Phytophthora* infection dynamics [26,31], we considered infection stages to be comparable between *M. polymorpha* and *N. benthamiana* infection time courses in the following layout: 1 dpi - 14 hpi; 2 dpi - 24 hpi; 3 dpi - 48 hpi; 4 dpi - 72 hpi).

QUANTIFICATION AND STATISTICAL ANALYSIS

Statistical details of experiments can be found in the corresponding figure legends. Here, the identity of the statistical tests used, the exact value of n (i.e. number of independently infected liverworts) and dispersion and precision measures are given (error bars represent mean +/- standard deviation, p-value cutoffs, etc.). All statistical analyses for transcriptomic and proteomic analyses are described in the methods details above. Statistical analysis of qRT-PCR expression data are described in figure legends and were performed using R.

SUPPLEMENTARY INFORMATION

Data S1. ***Marchantia-Phytophthora*** **RNA-sequencing analyses**

Transcriptomics data **related to Figures 1-4, Figure S2, and Data S3**. For sheets (1-4;6;7): significantly differentially expressed genes during *P. palmivora* infection (adjusted p-value < 10^{-3}, log fold change (|LFC| $\geqslant$ 2), variance-stabilised row-centered counts are shown. Time points represent days post infection (dpi).

Data S2. Proteomic analysis of the ***Marchantia-Phytophthora*** **interaction**

Proteomics data and comparisons to transcriptome data that is **related to Figure 1, Figure 2, Figure S1**. Significantly differentially abundant proteins/genes during *P. palmivora* infection are shown. Time points represent days post infection (dpi).

Data S3. ***Marchantia*** **DEG infection timecourse heatmaps**

Categorized heatmaps of *Marchantia* DEGs during the *Marchantia-Phytophthora* RNA-seq time course, **related to Figure 3 and Data S1**. 'Infected' indicates *P. palmivora* treatment while 'mock' represents treatment with water. d = days post treatment.

REFERENCES

1. Remy, W., Taylor, T.N., Hass, H., and Kerp, H. (1994). Four hundred-million-year-old vesicular arbuscular mycorrhizae. PNAS *91*, 11841–11843.
2. Taylor, T.N., Remy, W., Hass, H., and Kerp, H. (1995). Fossil arbuscular mycorrhizae from the Early Devonian. Mycologia *87*, 560–573.
3. Taylor, T.N., Krings, M., and Kerp, H. (2006). Hassiella monospora gen. et sp. nov., a microfungus from the 400 million year old Rhynie chert. Mycol. Res. *110*, 628–632.
4. Strullu-Derrien, C. (2018). Fossil filamentous microorganisms associated with plants in early terrestrial environments. Current Opinion in Plant Biology *44*, 122–128.
5. Krings, M., Taylor, T.N., Hass, H., Kerp, H., Dotzler, N., and Hermsen, E.J. (2007). Fungal endophytes in a 400-million-yr-old land plant: infection pathways, spatial distribution, and host responses. New Phytologist *174*, 648–657.
6. Boller, T., and Felix, G. (2009). A Renaissance of Elicitors: Perception of Microbe-Associated Molecular Patterns and Danger Signals by Pattern-Recognition Receptors. Annual Review of Plant Biology *60*, 379–406.
7. Macho, A.P., and Zipfel, C. (2014). Plant PRRs and the Activation of Innate Immune Signaling. Molecular Cell *54*, 263–272.
8. Cui, H., Tsuda, K., and Parker, J.E. (2015). Effector-Triggered Immunity: From Pathogen Perception to Robust Defense. Annual Review of Plant Biology *66*, 487–511.
9. Bednarek, P. (2012). Chemical warfare or modulators of defence responses – the function of secondary metabolites in plant immunity. Current Opinion in Plant Biology *15*, 407–414.
10. Meng, X., and Zhang, S. (2013). MAPK Cascades in Plant Disease Resistance Signaling. Annual Review of Phytopathology *51*, 245–266.
11. Morris, J.L., Puttick, M.N., Clark, J.W., Edwards, D., Kenrick, P., Pressel, S., Wellman, C.H., Yang, Z., Schneider, H., and Donoghue, P.C.J. (2018). The timescale of early land plant evolution. Proceedings of the National Academy of Sciences *115*, E2274–E2283.
12. Puttick, M.N., Morris, J.L., Williams, T.A., Cox, C.J., Edwards, D., Kenrick, P., Pressel, S., Wellman, C.H., Schneider, H., Pisani, D., *et al.* (2018). The Interrelationships of Land Plants and the Nature of the Ancestral Embryophyte. Current Biology *28*, 733-745.e2.
13. Sousa, F., Foster, P.G., Donoghue, P.C.J., Schneider, H., and Cox, C.J. (2019). Nuclear protein phylogenies support the monophyly of the three bryophyte groups (Bryophyta Schimp.). New Phytologist *222*, 565–575.
14. Rensing, S.A., Lang, D., Zimmer, A.D., Terry, A., Salamov, A., Shapiro, H., Nishiyama, T., Perroud, P.-F., Lindquist, E.A., Kamisugi, Y., *et al.* (2008). The Physcomitrella Genome Reveals Evolutionary Insights into the Conquest of Land by Plants. Science *319*, 64–69.
15. Bowman, J.L., Kohchi, T., Yamato, K.T., Jenkins, J., Shu, S., Ishizaki, K., Yamaoka, S., Nishihama, R., Nakamura, Y., Berger, F., *et al.* (2017). Insights into Land Plant Evolution Garnered from the Marchantia polymorpha Genome. Cell *171*, 287-304.e15.
16. Ponce de León, I., and Montesano, M. (2017). Adaptation Mechanisms in the Evolution of Moss Defenses to Microbes. Frontiers in Plant Science *8*. Available at: http://journal.frontiersin.org/article/10.3389/fpls.2017.00366/full [Accessed March 30, 2019].
17. Carella, P., and Schornack, S. (2018). Manipulation of Bryophyte Hosts by Pathogenic and Symbiotic Microbes. Plant and Cell Physiology *59*, 656–665.
18. de Vries, S., de Vries, J., von Dahlen, J.K., Gould, S.B., Archibald, J.M., Rose, L.E., and Slamovits, C.H. (2018). On plant defense signaling networks and early land plant evolution. Communicative & Integrative Biology *11*, 1–14.
19. Delaux, P.-M., Radhakrishnan, G.V., Jayaraman, D., Cheema, J., Malbreil, M., Volkening, J.D., Sekimoto, H., Nishiyama, T., Melkonian, M., Pokorny, L., *et al.* (2015). Algal ancestor

of land plants was preadapted for symbiosis. Proceedings of the National Academy of Sciences *112*, 13390–13395.
20. Field, K.J., and Pressel, S. (2018). Unity in diversity: structural and functional insights into the ancient partnerships between plants and fungi. New Phytologist *220*, 996–1011.
21. Bressendorff, S., Azevedo, R., Kenchappa, C.S., Ponce de León, I., Olsen, J.V., Rasmussen, M.W., Erbs, G., Newman, M.-A., Petersen, M., and Mundy, J. (2016). An Innate Immunity Pathway in the Moss *Physcomitrella patens*. The Plant Cell *28*, 1328–1342.
22. Reboledo, G., del Campo, R., Alvarez, A., Montesano, M., Mara, H., and Ponce de León, I. (2015). Physcomitrella patens Activates Defense Responses against the Pathogen Colletotrichum gloeosporioides. International Journal of Molecular Sciences *16*, 22280–22298.
23. Overdijk, E.J.R., De Keijzer, J., De Groot, D., Schoina, C., Bouwmeester, K., Ketelaar, T., and Govers, F. (2016). Interaction between the moss *Physcomitrella patens* and *Phytophthora* : a novel pathosystem for live-cell imaging of subcellular defence: INTERACTION BETWEEN *P. PATENS* AND *PHYTOPHTHORA*. Journal of Microscopy *263*, 171–180.
24. Monte, I., Ishida, S., Zamarreño, A.M., Hamberg, M., Franco-Zorrilla, J.M., García-Casado, G., Gouhier-Darimont, C., Reymond, P., Takahashi, K., García-Mina, J.M., *et al.* (2018). Ligand-receptor co-evolution shaped the jasmonate pathway in land plants. Nature Chemical Biology *14*, 480–488.
25. Nelson, J.M., Hauser, D.A., Hinson, R., and Shaw, A.J. (2018). A novel experimental system using the liverwort *Marchantia polymorpha* and its fungal endophytes reveals diverse and context-dependent effects. New Phytologist *218*, 1217–1232.
26. Carella, P., Gogleva, A., Tomaselli, M., Alfs, C., and Schornack, S. (2018). Phytophthora palmivora establishes tissue-specific intracellular infection structures in the earliest divergent land plant lineage. PNAS *115*, E3846–E3855.
27. van Loon, L.C., Pierpoint, W.S., Boller, Th., and Conejero, V. (1994). Recommendations for naming plant pathogenesis-related proteins. Plant Mol Biol Rep *12*, 245–264.
28. Sels, J., Mathys, J., De Coninck, B.M.A., Cammue, B.P.A., and De Bolle, M.F.C. (2008). Plant pathogenesis-related (PR) proteins: A focus on PR peptides. Plant Physiology and Biochemistry *46*, 941–950.
29. Ali, S., Ganai, B.A., Kamili, A.N., Bhat, A.A., Mir, Z.A., Bhat, J.A., Tyagi, A., Islam, S.T., Mushtaq, M., Yadav, P., *et al.* (2018). Pathogenesis-related proteins and peptides as promising tools for engineering plants with multiple stress tolerance. Microbiological Research *212–213*, 29–37.
30. Visser, E.A., Wegrzyn, J.L., Myburg, A.A., and Naidoo, S. (2018). Defence transcriptome assembly and pathogenesis related gene family analysis in Pinus tecunumanii (low elevation). BMC Genomics *19*. Available at: https://bmcgenomics.biomedcentral.com/articles/10.1186/s12864-018-5015-0 [Accessed March 30, 2019].
31. Evangelisti, E., Gogleva, A., Hainaux, T., Doumane, M., Tulin, F., Quan, C., Yunusov, T., Floch, K., and Schornack, S. (2017). Time-resolved dual transcriptomics reveal early induced Nicotiana benthamiana root genes and conserved infection-promoting Phytophthora palmivora effectors. BMC Biology *15*. Available at: http://bmcbiol.biomedcentral.com/articles/10.1186/s12915-017-0379-1 [Accessed March 30, 2019].
32. Emms, D.M., and Kelly, S. (2015). OrthoFinder: solving fundamental biases in whole genome comparisons dramatically improves orthogroup inference accuracy. Genome Biology *16*. Available at: http://genomebiology.com/2015/16/1/157 [Accessed March 30, 2019].

33. Liu, J., Osbourn, A., and Ma, P. (2015). MYB Transcription Factors as Regulators of Phenylpropanoid Metabolism in Plants. Molecular Plant *8*, 689–708.
34. Xu, W., Dubos, C., and Lepiniec, L. (2015). Transcriptional control of flavonoid biosynthesis by MYB–bHLH–WDR complexes. Trends in Plant Science *20*, 176–185.
35. Albert, N.W., Thrimawithana, A.H., McGhie, T.K., Clayton, W.A., Deroles, S.C., Schwinn, K.E., Bowman, J.L., Jordan, B.R., and Davies, K.M. (2018). Genetic analysis of the liverwort *Marchantia polymorpha* reveals that R2R3MYB activation of flavonoid production in response to abiotic stress is an ancient character in land plants. New Phytologist *218*, 554–566.
36. Clayton, W.A., Albert, N.W., Thrimawithana, A.H., McGhie, T.K., Deroles, S.C., Schwinn, K.E., Warren, B.A., McLachlan, A.R.G., Bowman, J.L., Jordan, B.R., *et al.* (2018). UVR8-mediated induction of flavonoid biosynthesis for UVB tolerance is conserved between the liverwort *Marchantia polymorpha* and flowering plants. The Plant Journal *96*, 503–517.
37. Kubo, H., Nozawa, S., Hiwatashi, T., Kondou, Y., Nakabayashi, R., Mori, T., Saito, K., Takanashi, K., Kohchi, T., and Ishizaki, K. (2018). Biosynthesis of riccionidins and marchantins is regulated by R2R3-MYB transcription factors in Marchantia polymorpha. Journal of Plant Research *131*, 849–864.
38. Nishihama, R., Ishida, S., Urawa, H., Kamei, Y., and Kohchi, T. (2016). Conditional Gene Expression/Deletion Systems for *Marchantia polymorpha* Using its Own Heat-Shock Promoter and Cre/ *lox* P-Mediated Site-Specific Recombination. Plant and Cell Physiology *57*, 271–280.
39. Ishizaki, K., Nishihama, R., Ueda, M., Inoue, K., Ishida, S., Nishimura, Y., Shikanai, T., and Kohchi, T. (2015). Development of Gateway Binary Vector Series with Four Different Selection Markers for the Liverwort Marchantia polymorpha. PLOS ONE *10*, e0138876.
40. Oliver, J.P., Castro, A., Gaggero, C., Cascón, T., Schmelz, E.A., Castresana, C., and Ponce de León, I. (2009). Pythium infection activates conserved plant defense responses in mosses. Planta *230*, 569–579.
41. Castro, A., Vidal, S., and Ponce de León, I. (2016). Moss Pathogenesis-Related-10 Protein Enhances Resistance to Pythium irregulare in Physcomitrella patens and Arabidopsis thaliana. Frontiers in Plant Science *7*. Available at: http://journal.frontiersin.org/Article/10.3389/fpls.2016.00580/abstract [Accessed March 30, 2019].
42. de Vries, S., de Vries, J., Teschke, H., von Dahlen, J.K., Rose, L.E., and Gould, S.B. (2018). Jasmonic and salicylic acid response in the fern *Azolla filiculoides* and its cyanobiont: Jasmonic and salicylic acid response in Azolla. Plant, Cell & Environment *41*, 2530–2548.
43. Winter, P.S., Bowman, C.E., Villani, P.J., Dolan, T.E., and Hauck, N.R. (2014). Systemic Acquired Resistance in Moss: Further Evidence for Conserved Defense Mechanisms in Plants. PLOS ONE *9*, e101880.
44. Hirsch, S., and Oldroyd, G.E.D. (2009). GRAS-domain transcription factors that regulate plant development. Plant Signaling & Behavior *4*, 698–700.
45. Grosche, C., Genau, A.C., and Rensing, S.A. (2018). Evolution of the Symbiosis-Specific GRAS Regulatory Network in Bryophytes. Frontiers in Plant Science *9*. Available at: https://www.frontiersin.org/article/10.3389/fpls.2018.01621/full [Accessed March 30, 2019].
46. Rey, T., Bonhomme, M., Chatterjee, A., Gavrin, A., Toulotte, J., Yang, W., André, O., Jacquet, C., and Schornack, S. (2017). The Medicago truncatula GRAS protein RAD1 supports arbuscular mycorrhiza symbiosis and Phytophthora palmivora susceptibility. Journal of Experimental Botany *68*, 5871–5881.
47. Vigneron, N., Radhakrishnan, G.V., and Delaux, P.-M. (2018). What have we learnt from studying the evolution of the arbuscular mycorrhizal symbiosis? Current Opinion in Plant Biology *44*, 49–56.

48. Pandey, S.P., and Somssich, I.E. (2009). The Role of WRKY Transcription Factors in Plant Immunity. PLANT PHYSIOLOGY *150*, 1648–1655.
49. Rushton, P.J., Somssich, I.E., Ringler, P., and Shen, Q.J. (2010). WRKY transcription factors. Trends in Plant Science *15*, 247–258.
50. Sarris, P.F., Duxbury, Z., Huh, S.U., Ma, Y., Segonzac, C., Sklenar, J., Derbyshire, P., Cevik, V., Rallapalli, G., Saucet, S.B., *et al.* (2015). A Plant Immune Receptor Detects Pathogen Effectors that Target WRKY Transcription Factors. Cell *161*, 1089–1100.
51. Sarris, P.F., Cevik, V., Dagdas, G., Jones, J.D.G., and Krasileva, K.V. (2016). Comparative analysis of plant immune receptor architectures uncovers host proteins likely targeted by pathogens. BMC Biology *14*. Available at: http://bmcbiol.biomedcentral.com/articles/10.1186/s12915-016-0228-7 [Accessed March 30, 2019].
52. Dixon, R.A., Achnine, L., Kota, P., Liu, C.-J., Reddy, M.S.S., and Wang, L. (2002). The phenylpropanoid pathway and plant defence-a genomics perspective. Molecular Plant Pathology *3*, 371–390.
53. Naoumkina, M.A., Zhao, Q., Gallego-Giraldo, L., Dai, X., Zhao, P.X., and Dixon, R.A. (2010). Genome-wide analysis of phenylpropanoid defence pathways: Phenylpropanoid defence pathways. Molecular Plant Pathology, no-no.
54. Falcone Ferreyra, M.L., Rius, S.P., and Casati, P. (2012). Flavonoids: biosynthesis, biological functions, and biotechnological applications. Frontiers in Plant Science *3*. Available at: http://journal.frontiersin.org/article/10.3389/fpls.2012.00222/abstract [Accessed March 30, 2019].
55. Alvarez, A., Montesano, M., Schmelz, E., and Ponce de León, I. (2016). Activation of Shikimate, Phenylpropanoid, Oxylipins, and Auxin Pathways in Pectobacterium carotovorum Elicitors-Treated Moss. Frontiers in Plant Science *7*. Available at: http://journal.frontiersin.org/Article/10.3389/fpls.2016.00328/abstract [Accessed March 30, 2019].
56. Cushnie, T.P.T., and Lamb, A.J. (2005). Antimicrobial activity of flavonoids. Int. J. Antimicrob. Agents *26*, 343–356.
57. Cisowska, A., Wojnicz, D., and Hendrich, A.B. (2011). Anthocyanins as antimicrobial agents of natural plant origin. Nat Prod Commun *6*, 149–156.
58. Piasecka, A., Jedrzejczak-Rey, N., and Bednarek, P. (2015). Secondary metabolites in plant innate immunity: conserved function of divergent chemicals. New Phytologist *206*, 948–964.
59. Renault, H., Alber, A., Horst, N.A., Basilio Lopes, A., Fich, E.A., Kriegshauser, L., Wiedemann, G., Ullmann, P., Herrgott, L., Erhardt, M., *et al.* (2017). A phenol-enriched cuticle is ancestral to lignin evolution in land plants. Nature Communications *8*, 14713.
60. Paniagua, C., Bilkova, A., Jackson, P., Dabravolski, S., Riber, W., Didi, V., Houser, J., Gigli-Bisceglia, N., Wimmerova, M., Budínská, E., *et al.* (2017). Dirigent proteins in plants: modulating cell wall metabolism during abiotic and biotic stress exposure. Journal of Experimental Botany *68*, 3287–3301.
61. Wu, Y.-F., Zhao, Y., Liu, X.-Y., Gao, S., Cheng, A.-X., and Lou, H.-X. (2018). A bHLH Transcription Factor Regulates Bisbibenzyl Biosynthesis in the Liverwort Plagiochasma appendiculatum. Plant and Cell Physiology *59*, 1187–1199.
62. Lillo, C., Lea, U.S., and Ruoff, P. (2008). Nutrient depletion as a key factor for manipulating gene expression and product formation in different branches of the flavonoid pathway. Plant, Cell & Environment *31*, 587–601.
63. Shan, X., Zhang, Y., Peng, W., Wang, Z., and Xie, D. (2009). Molecular mechanism for jasmonate-induction of anthocyanin accumulation in Arabidopsis. Journal of Experimental Botany *60*, 3849–3860.

64. Li, S., Wang, W., Gao, J., Yin, K., Wang, R., Wang, C., Petersen, M., Mundy, J., and Qiu, J.-L. (2016). MYB75 Phosphorylation by MPK4 Is Required for Light-Induced Anthocyanin Accumulation in Arabidopsis. The Plant Cell *28*, 2866–2883.
65. Wersch, R. van, Gao, F., and Zhang, Y. (2018). Mitogen-activated protein kinase kinase 6 negatively regulates anthocyanin induction in Arabidopsis. Plant Signaling & Behavior *13*, e1526000.
66. Boter, M., Golz, J.F., Giménez-Ibañez, S., Fernandez-Barbero, G., Franco-Zorrilla, J.M., and Solano, R. (2015). FILAMENTOUS FLOWER Is a Direct Target of JAZ3 and Modulates Responses to Jasmonate. The Plant Cell *27*, 3160–3174.
67. de Vries, J., de Vries, S., Slamovits, C.H., Rose, L.E., and Archibald, J.M. (2017). How Embryophytic is the Biosynthesis of Phenylpropanoids and their Derivatives in Streptophyte Algae? Plant and Cell Physiology *58*, 934–945.
68. de Vries, J., Curtis, B.A., Gould, S.B., and Archibald, J.M. (2018). Embryophyte stress signaling evolved in the algal progenitors of land plants. Proceedings of the National Academy of Sciences *115*, E3471–E3480.
69. Tohge, T., Watanabe, M., Hoefgen, R., and Fernie, A.R. (2013). The evolution of phenylpropanoid metabolism in the green lineage. Critical Reviews in Biochemistry and Molecular Biology *48*, 123–152.
70. Upson, J.L., Zess, E.K., Białas, A., Wu, C., and Kamoun, S. (2018). The coming of age of EvoMPMI: evolutionary molecular plant–microbe interactions across multiple timescales. Current Opinion in Plant Biology *44*, 108–116.
71. Le Fevre, R., O'Boyle, B., Moscou, M.J., and Schornack, S. (2016). Colonization of Barley by the Broad-Host Hemibiotrophic Pathogen *Phytophthora palmivora* Uncovers a Leaf Development–Dependent Involvement of *Mlo*. Molecular Plant-Microbe Interactions *29*, 385–395.
72. Ah-Fong, A.M.V., and Judelson, H.S. (2011). Vectors for fluorescent protein tagging in Phytophthora: tools for functional genomics and cell biology. Fungal Biology *115*, 882–890.
73. Rey, T., Chatterjee, A., Buttay, M., Toulotte, J., and Schornack, S. (2015). *Medicago truncatula* symbiosis mutants affected in the interaction with a biotrophic root pathogen. New Phytologist *206*, 497–500.
74. Koressaar, T., and Remm, M. (2007). Enhancements and modifications of primer design program Primer3. Bioinformatics *23*, 1289–1291.
75. Untergasser, A., Cutcutache, I., Koressaar, T., Ye, J., Faircloth, B.C., Remm, M., and Rozen, S.G. (2012). Primer3—new capabilities and interfaces. Nucleic Acids Research *40*, e115–e115.
76. Saint-Marcoux, D., Proust, H., Dolan, L., and Langdale, J.A. (2015). Identification of Reference Genes for Real-Time Quantitative PCR Experiments in the Liverwort Marchantia polymorpha. PLOS ONE *10*, e0118678.
77. Borner, G.H.H., and Fielding, A.B. (2014). Using In-Solution Digestion, Peptide Fractionation, and a Q Exactive Mass Spectrometer to Analyze the Proteome of Clathrin-Coated Vesicles. Cold Spring Harbor Protocols *2014*, pdb.prot084137.
78. Cox, J., and Mann, M. (2008). MaxQuant enables high peptide identification rates, individualized p.p.b.-range mass accuracies and proteome-wide protein quantification. Nature Biotechnology *26*, 1367–1372.
79. Tyanova, S., Temu, T., and Cox, J. (2016). The MaxQuant computational platform for mass spectrometry-based shotgun proteomics. Nat Protoc *11*, 2301–2319.
80. Ali, S.S., Shao, J., Lary, D.J., Kronmiller, B.A., Shen, D., Strem, M.D., Amoako-Attah, I., Akrofi, A.Y., Begoude, B.A.D., ten Hoopen, G.M., *et al.* (2017). Phytophthora megakarya and Phytophthora palmivora, Closely Related Causal Agents of Cacao Black Pod Rot, Underwent Increases in Genome Sizes and Gene Numbers by Different Mechanisms. Genome Biology and Evolution *9*, 536–557.

81. Kubota, A., Ishizaki, K., Hosaka, M., and Kohchi, T. (2013). Efficient *Agrobacterium* - Mediated Transformation of the Liverwort *Marchantia polymorpha* Using Regenerating Thalli. Bioscience, Biotechnology, and Biochemistry *77*, 167–172.
82. Dobin, A., Davis, C.A., Zaleski, C., Schlesinger, F., Drenkow, J., Chaisson, M., Batut, P., Jha, S., and Gingeras, T.R. (2012). STAR: ultrafast universal RNA-seq aligner. Bioinformatics *29*, 15–21.
83. Liao, Y., Smyth, G.K., and Shi, W. (2014). featureCounts: an efficient general purpose program for assigning sequence reads to genomic features. Bioinformatics *30*, 923–930.
84. Love, M.I., Huber, W., and Anders, S. (2014). Moderated estimation of fold change and dispersion for RNA-seq data with DESeq2. Genome Biology *15*. Available at: http://genomebiology.biomedcentral.com/articles/10.1186/s13059-014-0550-8 [Accessed March 30, 2019].

KEY RESOURCES TABLE

REAGENT or RESOURCE	SOURCE	IDENTIFIER
Bacterial and Virus Strains		
E. coli TOP10 chemically competent cells	Invitrogen	Cat#C404006
Agrobacterium tumefaciens GV3101 (pMP90)	Our laboratory collection	N/A
Chemicals, Peptides, and Recombinant Proteins		
PureLink Plant RNA Reagent	ThermoFisher	Cat#12322012
SuperScript II reverse transcriptase	ThermoFisher	Cat#18064014
RNAse OUT ribonuclease inhibitor	ThermoFisher	Cat#10777019
Roche SYBR mix	Roche Life Science	Cat#4887352001
Gateway LR clonase II enzyme mix	ThermoFisher	Cat#11791020
MS-media + B5	Duchefa Biochemie	Cat#M0231
Plant agar	Duchefa Biochemie	Cat#P1001
Cefotaxime sodium salt	Sigma-Aldrich	Cat#C7039
Hygromycin B	Melford	Cat#H7502
Chlorsulfuron	Sigma-Aldrich	Cat#34322
G418	Melford	Cat#G0175
carbenicillin	Sigma-Aldrich	Cat#C3416
X-GlcA	Melford	Cat#MB1021
Propidium iodide	Sigma-Aldrich	Cat#P4170
Phosphatase Inhibitor Cocktail 3	Sigma-Aldrich	Cat#P0044-5ML
Phosphatase Inhibitor Cocktail 2	Sigma-Aldrich	Cat#P5726-5ML
Critical Commercial Assays		
QIAprep spin miniprep kit	Qiagen	Cat#27106
Turbo DNA-free kit	Invitrogen	Cat#AM1907
TruSeq RNA Library Prep Kit v2	Illumina	Cat#RS-122-2001
Deposited Data		
Raw sequencing data: *Marchantia polymorpha*	This study	NCBI SRA, PRJNA397637
Raw sequencing data: *Nicotiana benthamiana*	This study	NCBI SRA, PRJNA503573
Marchantia polymorpha reference genome v3.1	[15]	http://marchantia.info/
Nicotiana benthamiana reference genome v1.0.1	SolGenomics Network	https://solgenomics.net/organism/Nicotiana_benthamiana/genome
Phytophthora palmivora reference proteome	[80]	BioProject, PRJNA318026
Raw proteomics data	This study	PRIDE, PXD012076
Experimental Models: Organisms/Strains		
Marchantia polymorpha TAK1	Prof. Jim Haseloff, University of Cambridge	N/A
$_{pro}$Mp*PR6a:GUS*	This study	N/A
$_{pro}$Mp*PR6a:tdTomato-NLS*	This study	N/A
$_{pro}$Mp*PRX:tdTomato-NLS*	This study	N/A

pro35S:mCitrine-FLAG-MpMyb14	This study	N/A
*proHSP:FLAG-*Mp*Myb14*	This study	N/A
Mp*myb14-202f*	[37]	N/A
Mp*myb14-455r*	[37]	N/A
Nicotiana benthamiana	Our laboratory collection	N/A
Phytophthora palmivora ARI-tdTomato	[71]	N/A
Phytophthora palmivora ARI-GFP	This study	N/A
Phytophthora palmivora LILI-YFP-KDEL	[31]	N/A
Oligonucleotides		
A list of all oligonucleotides used in this study can be found in Table S1	This study	N/A
Recombinant DNA		
pMpGWB104	[39]	Addgene Cat#68558
pMpGWB105	[39]	Addgene Cat#68559
pMpGW132	[39]	Addgene Cat#68586
pMpGWB316	[39]	Addgene Cat#68644
*pro*Mp*PR6a:tdTomato-NLS*	This study	N/A
*pro*Mp*PR6a:GUS*	This study	N/A
*pro*Mp*PRX:tdTomato-NLS*	This study	N/A
*pro35S:FLAG-*Mp*Myb14*	This study	N/A
*proHSP:FLAG-*Mp*Myb14*	This study	N/A
pENTR-proMpPRX	[26]	N/A
pENTR-FLAG-MpMyb14-CO	This study	GenBank, MK835684
pENTR-proMpPR6a	This study	GenBank, MK835683
Software and Algorithms		
ImageJ (Fiji)	https://imagej.net/Fiji/Downloads	Version: 2.0.0-rc-62/1.51s
Microsoft Powerpoint	Microsoft	Version 16.16.8
Prism 6.0	Graph-Pad	https://www.graphpad.com/
Rstudio	https://www.rstudio.com/	V1.1.383
Primer3	[74,75]	http://primer3.ut.ee/
MaxQuant version 1.5.7.4,	[78]	http://www.maxquant.org/)
Perseus version 1.5.8.5,	[79]	http://www.maxquant.org/).
OrthoFinder	[32]	https://github.com/davidemms/OrthoFinder
R package “pheatmap”	R. Kolde	https://github.com/raivokolde/pheatmap
R packages “alluvial”	Bojanowski and Edwards	https://cran.r-project.org/web/packages/alluvial/index.html
FastQC	Babraham Bioinformatics	https://www.bioinformatics.babraham.ac.uk/projects/fastqc/

DESeq2	[84]	https://bioconductor.org/packages/release/bioc/html/DESeq2.html
STAR aligner	[82]	https://github.com/alexdobin/STAR
FeatureCounts	[83]	http://bioinf.wehi.edu.au/featureCounts/

Figure 1

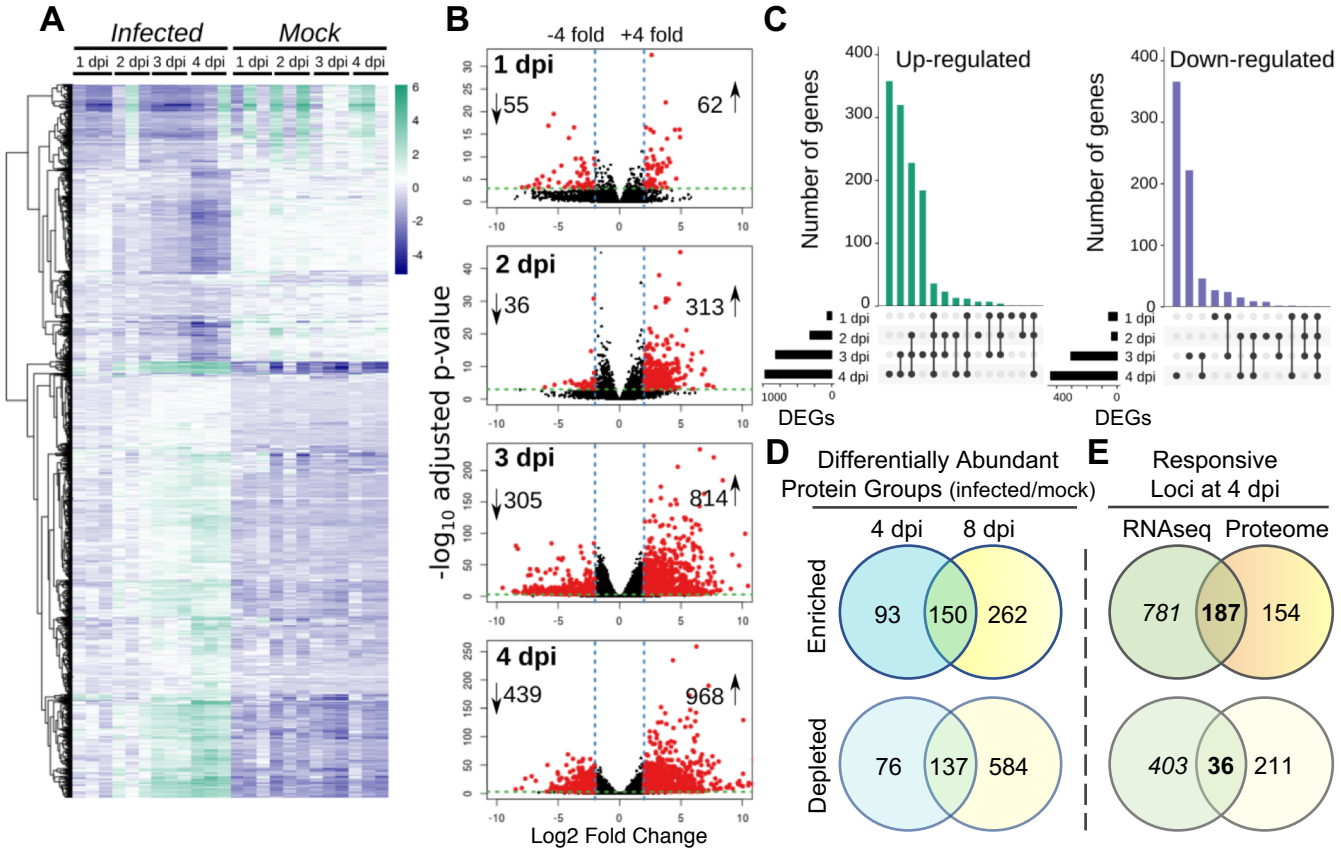
A
Infected
Mock
1 dpi 2 dpi 3 dpi 4 dpi 1 dpi 2 dpi 3 dpi 4 dpi
B
-4 fold +4 fold
1 dpi
55
62
2 dpi
36
313
3 dpi
305
814
4 dpi
439
968
-log10 adjusted p-value
Log2 Fold Change
C
Up-regulated
Down-regulated
Number of genes
1 dpi
2 dpi
3 dpi
4 dpi
DEGs
D
Differentially Abundant
Protein Groups (infected/mock)
4 dpi
8 dpi
Enriched
93
150
262
Depleted
76
137
584
E
Responsive
Loci at 4 dpi
RNAseq
Proteome
781
187
154
403
36
211

Figure 2

A

PR Family	Description	Induced* by *P. palmivora*
PR1	Cysteine-rich secreted	1
PR2	β-Glucanase	3
PR3	Chitinase	1
PR5	Thaumatin-like	1
PR6	Protease inhibitor	3
PR9	Peroxidase	14
PR15	Cupin	12

* = upregulated during infection in transcriptome & proteome at 4 dpi

B

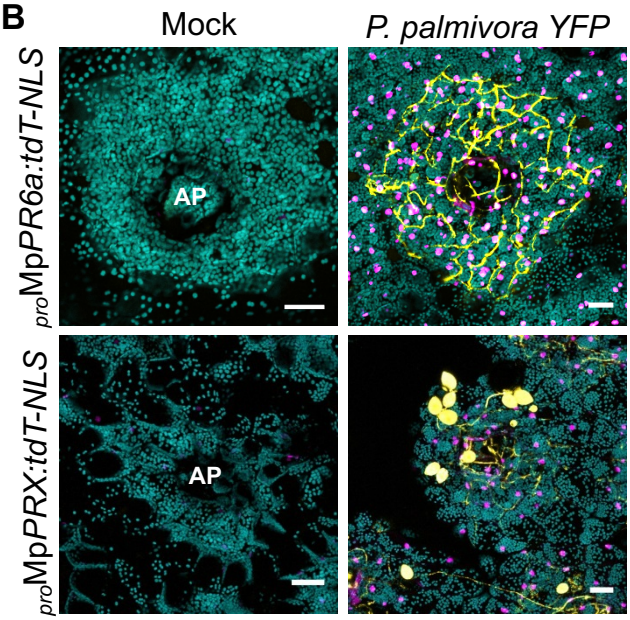

C

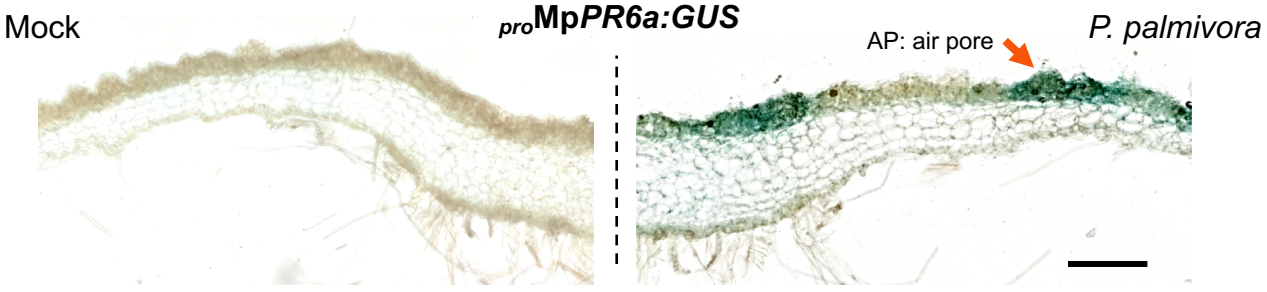

Figure 3

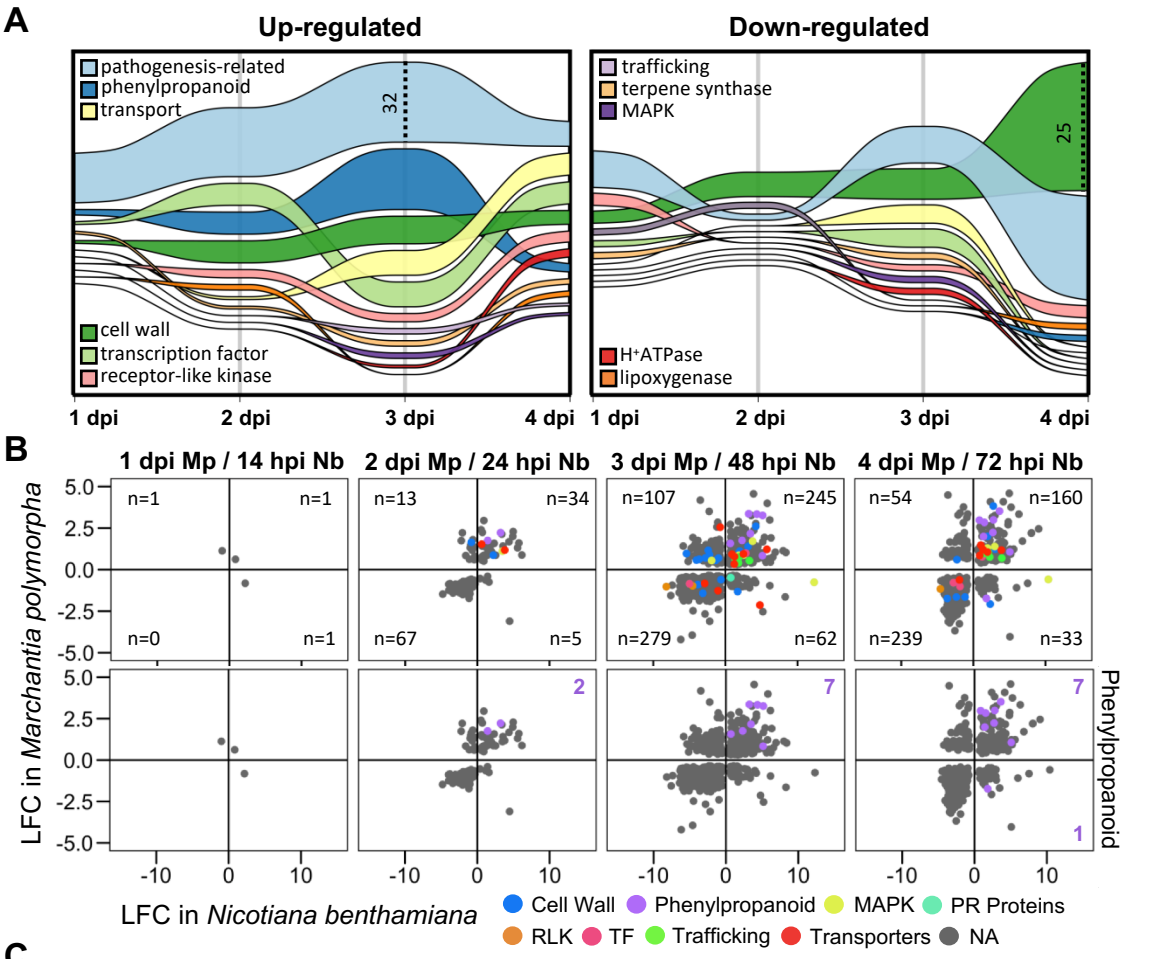
A
Up-regulated
Down-regulated
pathogenesis-related
phenylpropanoid
transport
cell wall
transcription factor
receptor-like kinase
32
trafficking
terpene synthase
MAPK
H+ATPase
lipoxygenase
25
1 dpi
2 dpi
3 dpi
4 dpi
B
1 dpi Mp / 14 hpi Nb
2 dpi Mp / 24 hpi Nb
3 dpi Mp / 48 hpi Nb
4 dpi Mp / 72 hpi Nb
LFC in Marchantia polymorpha
Phenylpropanoid
LFC in Nicotiana benthamiana
Cell Wall
Phenylpropanoid
MAPK
PR Proteins
RLK
TF
Trafficking
Transporters
NA
C
Marchantia-Phytophthora
Nicotiana-Phytophthora
14 hpi
24 hpi
48 hpi
72 hpi
Phenylpropanoid Orthologs
OG0006696 3-Dehydroquinate synthase
OG0007090 DAH7PS
OG0005470 3-Ketoacyl-CoA synthase
OG0006728 Arogenate dehydratase
OG0006208 Chorismate mutase
OG0006644 Chorismate synthase
OG0005996 Cinnamate 4'-hydroxylase
OG0005280 Coumarate 3'-hydroxylase
OG0005924 Phenylalanine ammonia lyase

Figure 4

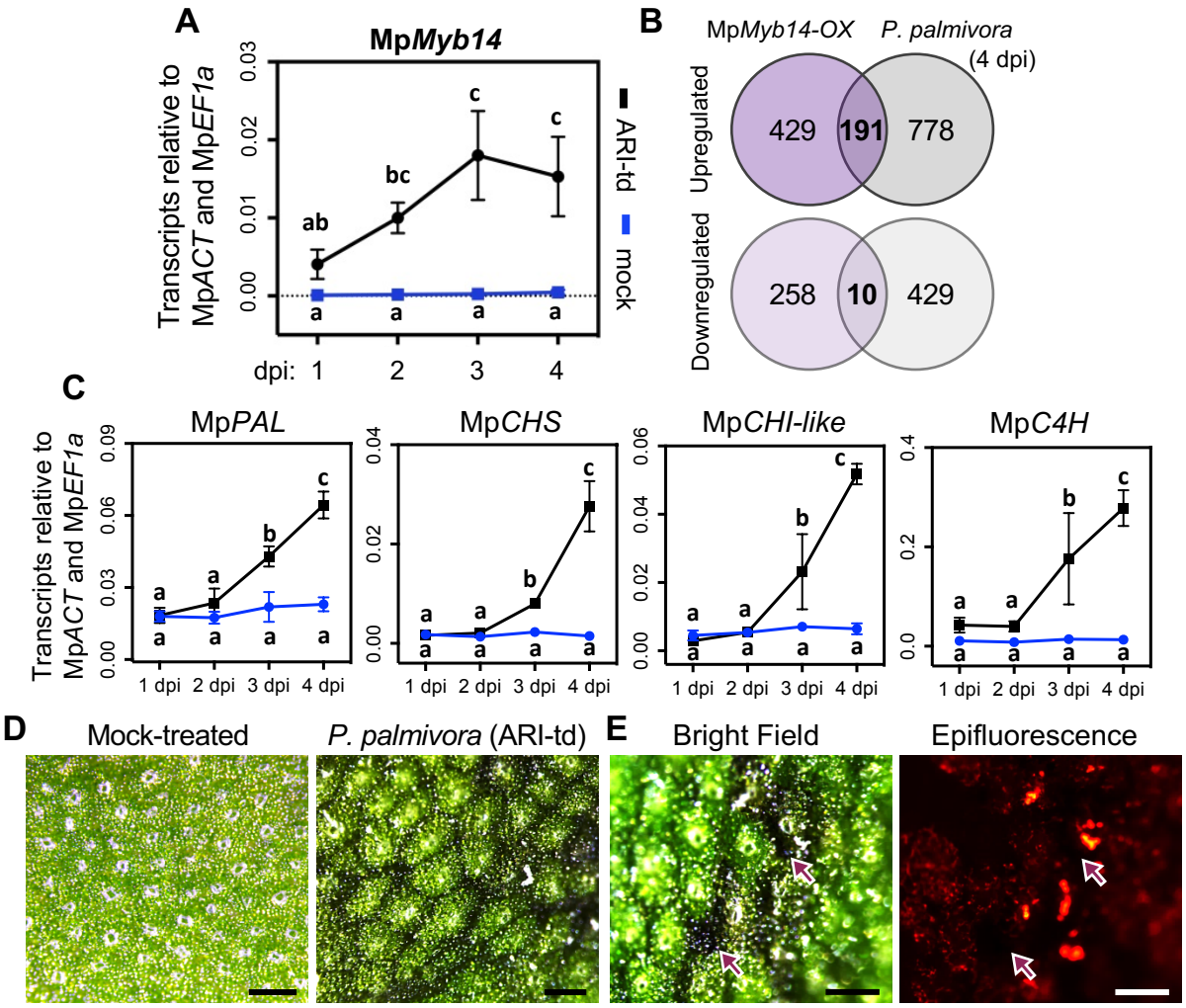
A
Mp*Myb14*
Transcripts relative to Mp*ACT* and Mp*EF1a*
0.00
0.01
0.02
0.03
ab
bc
c
c
a
a
a
a
dpi: 1 2 3 4
ARI-td
mock
B
Mp*Myb14-OX*
P. palmivora (4 dpi)
Upregulated
Downregulated
429
191
778
258
10
429
C
Mp*PAL*
Mp*CHS*
Mp*CHI-like*
Mp*C4H*
Transcripts relative to Mp*ACT* and Mp*EF1a*
1 dpi 2 dpi 3 dpi 4 dpi
D
Mock-treated
P. palmivora (ARI-td)
E
Bright Field
Epifluorescence

Figure 5

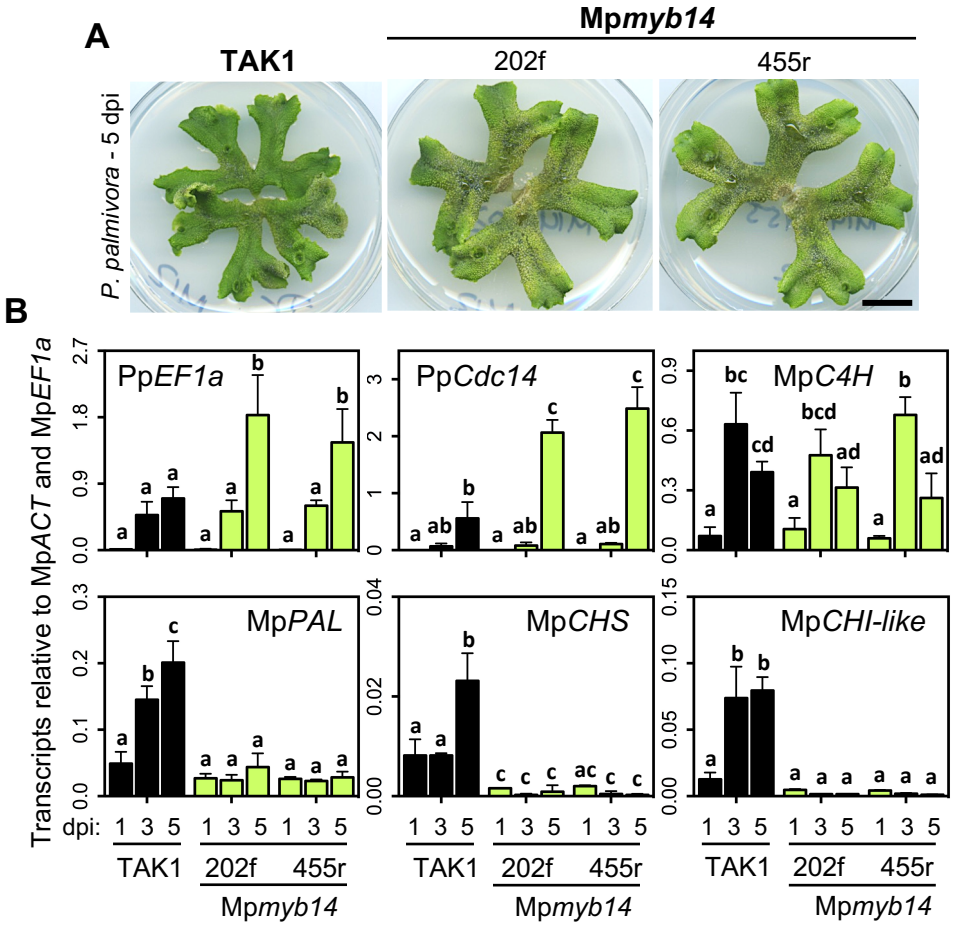
A
Mpmyb14
TAK1
202f
455r
P. palmivora - 5 dpi
B
Transcripts relative to MpACT and MpEF1a
PpEF1a
PpCdc14
MpC4H
MpPAL
MpCHS
MpCHI-like
dpi: 1 3 5 1 3 5 1 3 5
TAK1
202f
455r
Mpmyb14

Figure 6

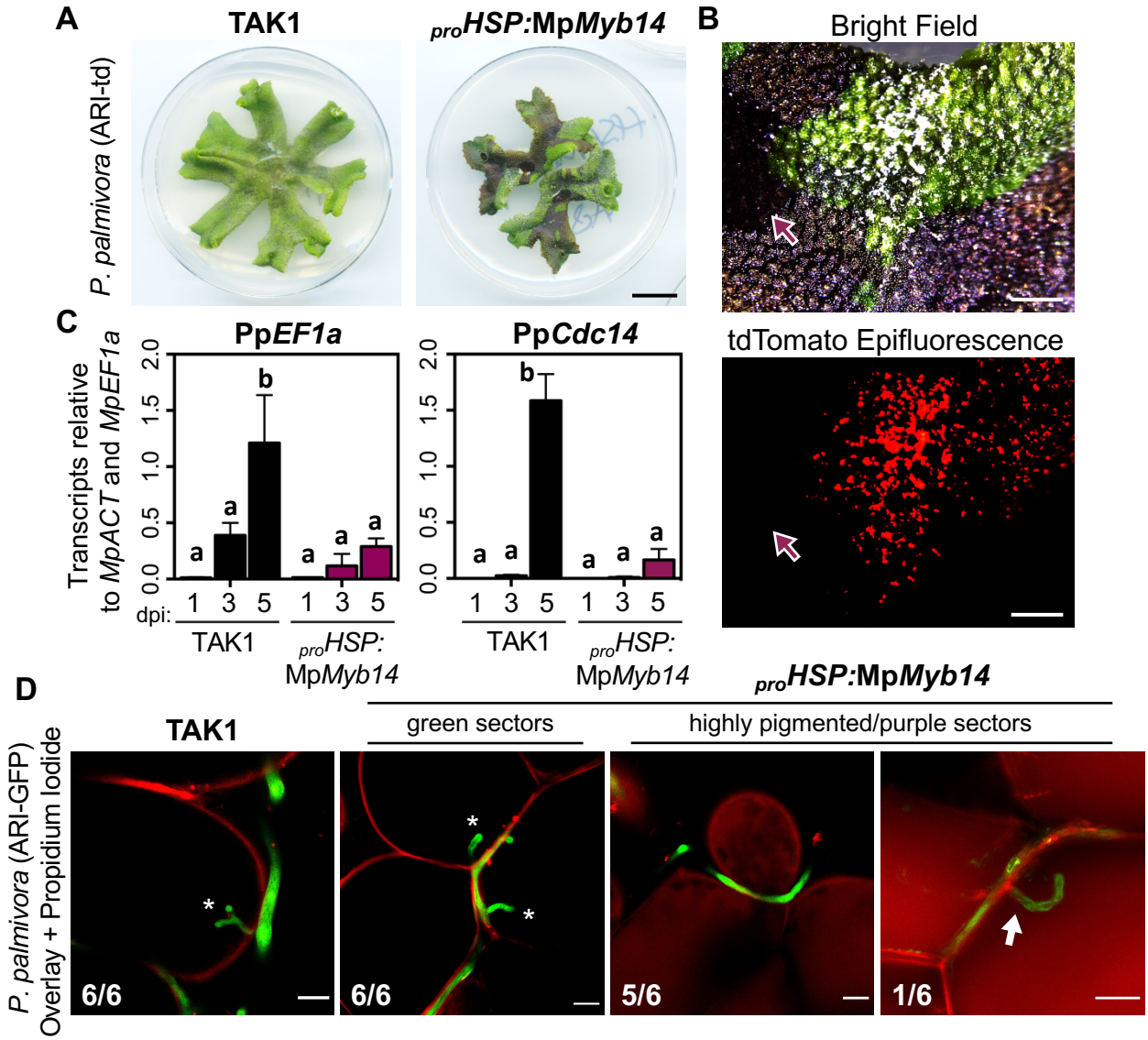
A
TAK1
proHSP:MpMyb14
P. palmivora (ARI-td)
B
Bright Field
tdTomato Epifluorescence
C
PpEF1a
PpCdc14
Transcripts relative to MpACT and MpEF1a
dpi: 1 3 5 1 3 5
TAK1
proHSP: MpMyb14
D
TAK1
proHSP:MpMyb14
green sectors
highly pigmented/purple sectors
P. palmivora (ARI-GFP) Overlay + Propidium Iodide
6/6
6/6
5/6
1/6

RLKs

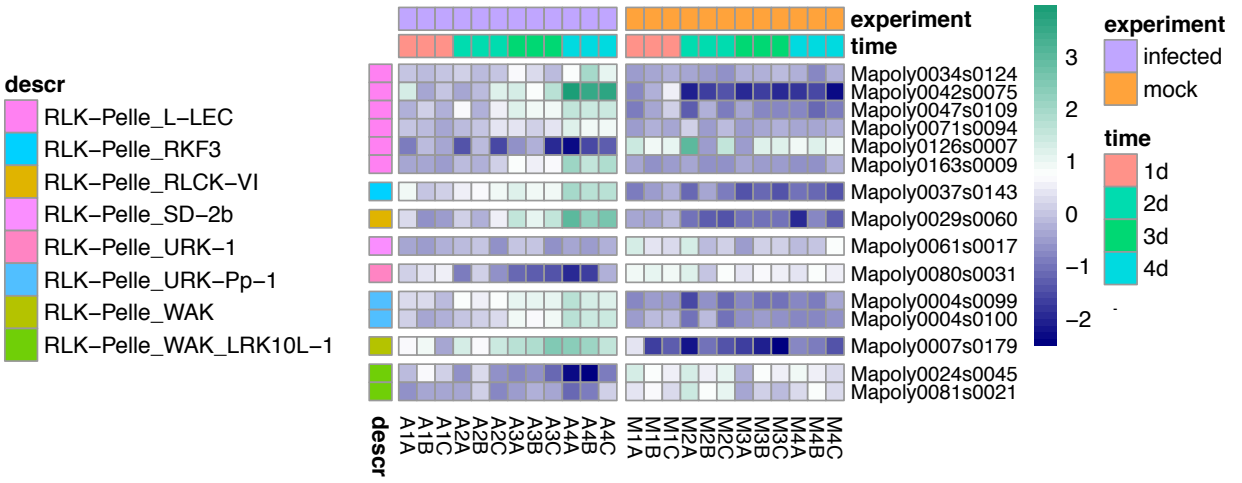

Phenylpropanoid/Flavonoid Pathway

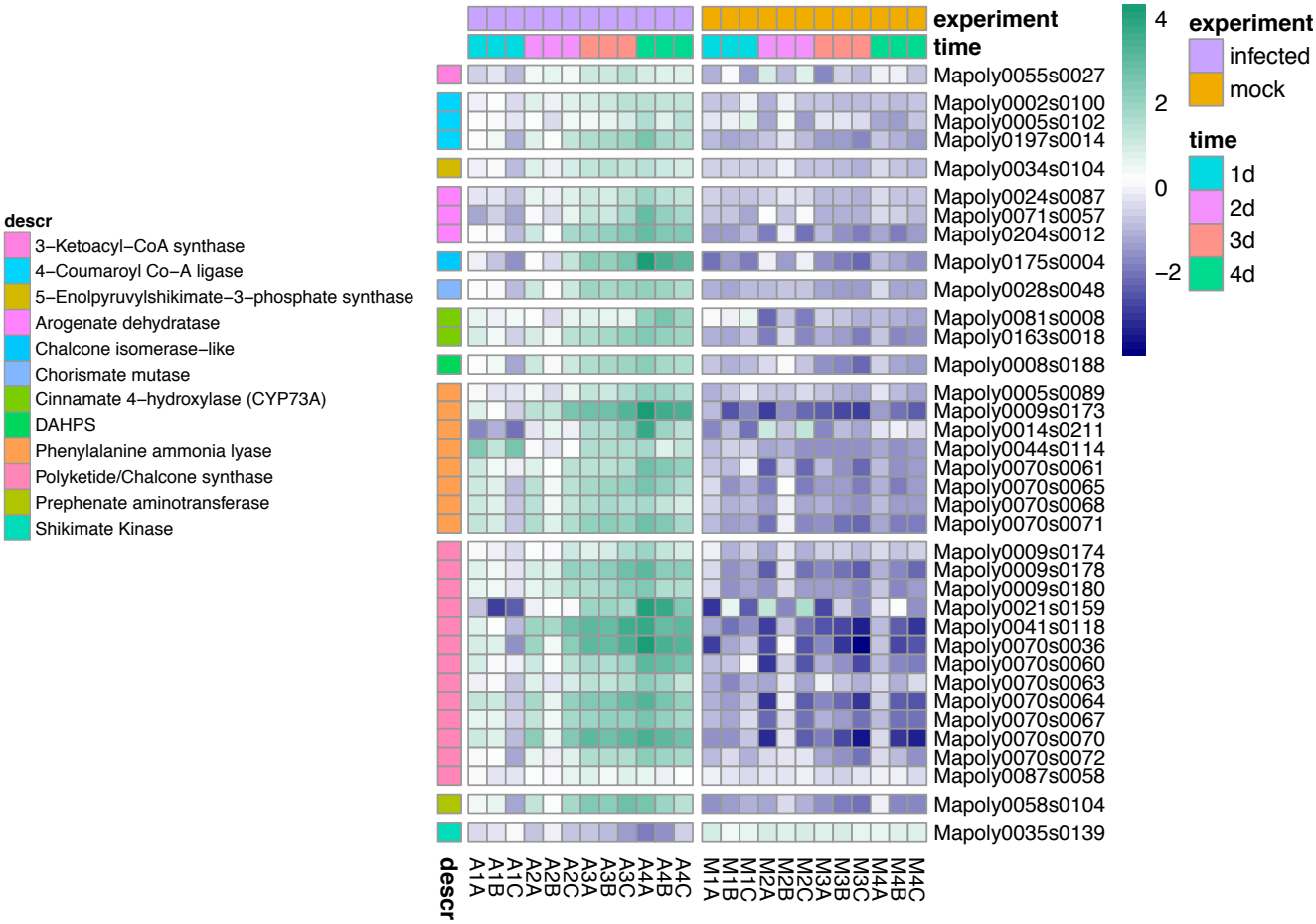

MAPKs

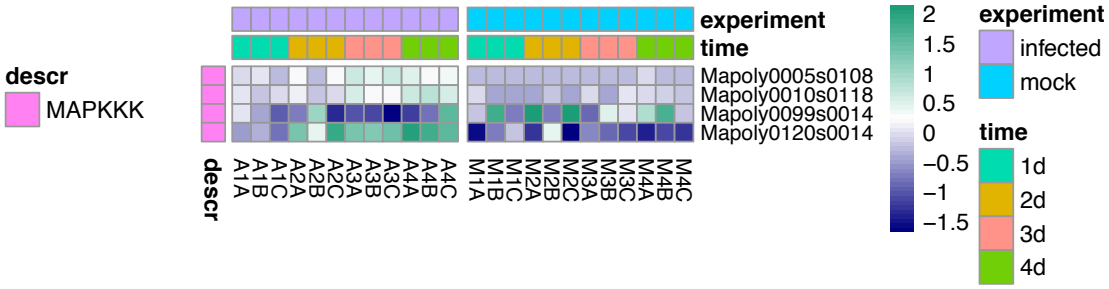

H+ATPases

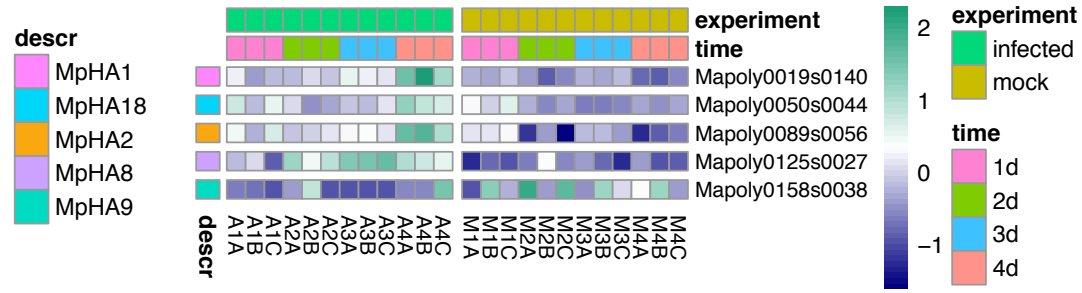

LOX

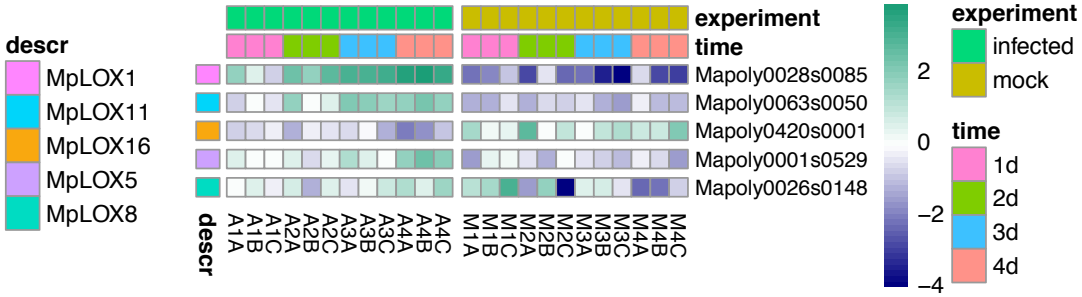

Trafficking

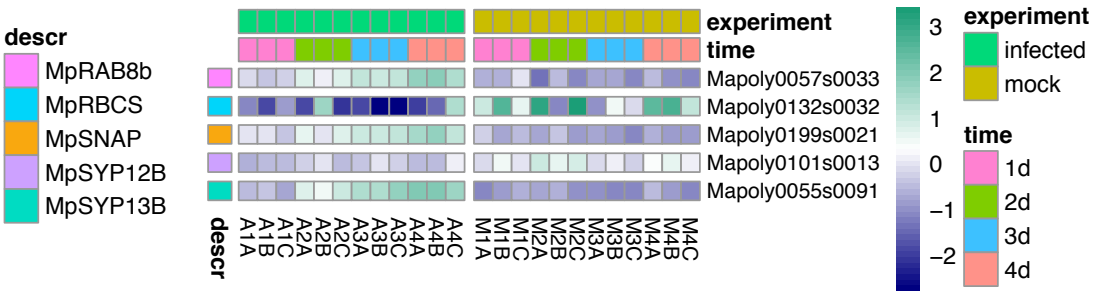

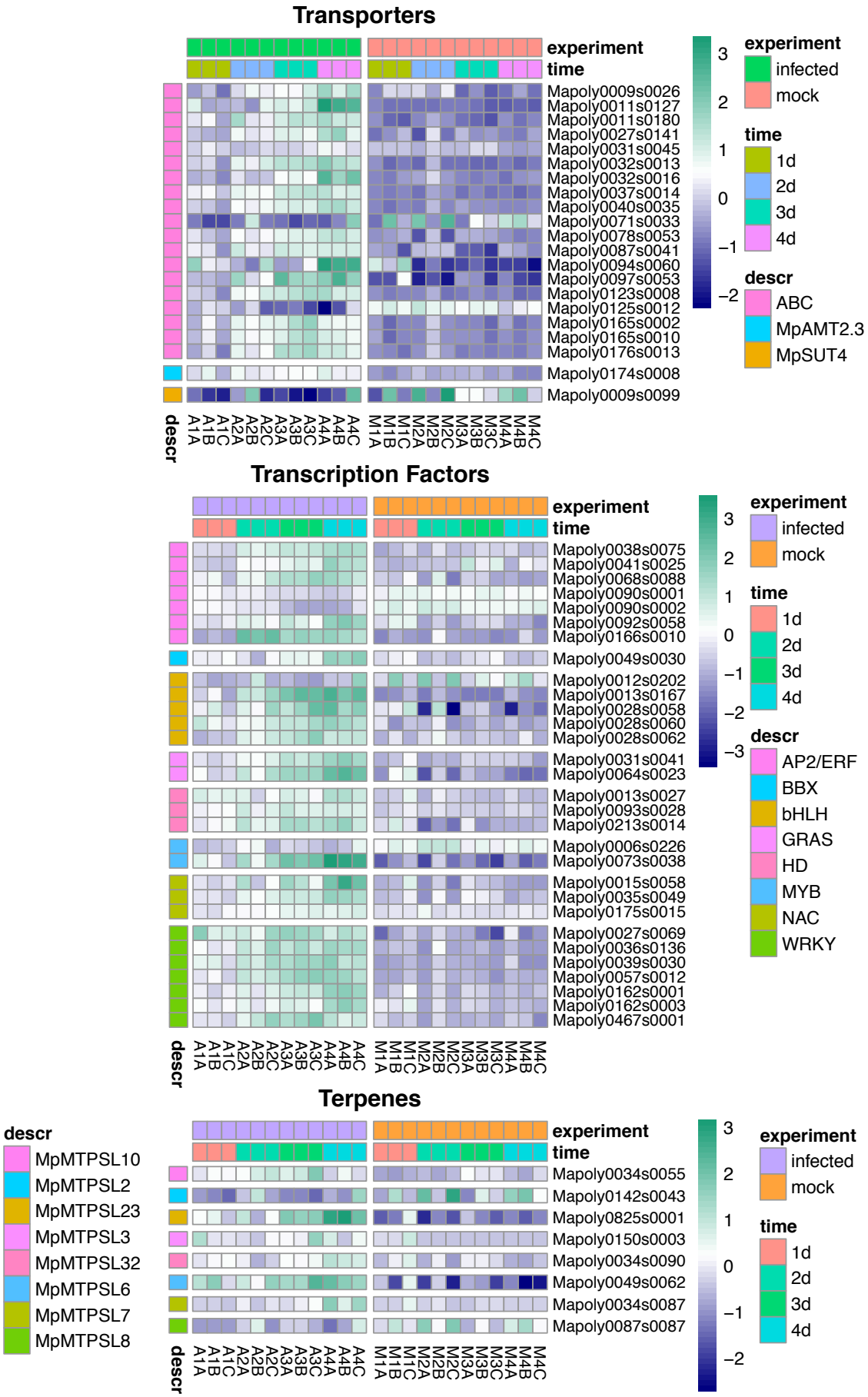
Transporters
experiment
time
Mapoly0009s0026
Mapoly0011s0127
Mapoly0011s0180
Mapoly0027s0141
Mapoly0031s0045
Mapoly0032s0013
Mapoly0032s0016
Mapoly0037s0014
Mapoly0040s0035
Mapoly0071s0033
Mapoly0078s0053
Mapoly0087s0041
Mapoly0094s0060
Mapoly0097s0053
Mapoly0123s0008
Mapoly0125s0012
Mapoly0165s0002
Mapoly0165s0010
Mapoly0176s0013
Mapoly0174s0008
Mapoly0009s0099
descr
A1A A1B A1C A2A A2B A2C A3A A3B A3C A4A A4B A4C M1A M1B M1C M2A M2B M2C M3A M3B M3C M4A M4B M4C
3 2 1 0 −1 −2
experiment
infected
mock
time
1d
2d
3d
4d
descr
ABC
MpAMT2.3
MpSUT4
Transcription Factors
experiment
time
Mapoly0038s0075
Mapoly0041s0025
Mapoly0068s0088
Mapoly0090s0001
Mapoly0090s0002
Mapoly0092s0058
Mapoly0166s0010
Mapoly0049s0030
Mapoly0012s0202
Mapoly0013s0167
Mapoly0028s0058
Mapoly0028s0060
Mapoly0028s0062
Mapoly0031s0041
Mapoly0064s0023
Mapoly0013s0027
Mapoly0093s0028
Mapoly0213s0014
Mapoly0006s0226
Mapoly0073s0038
Mapoly0015s0058
Mapoly0035s0049
Mapoly0175s0015
Mapoly0027s0069
Mapoly0036s0136
Mapoly0039s0030
Mapoly0057s0012
Mapoly0162s0001
Mapoly0162s0003
Mapoly0467s0001
descr
A1A A1B A1C A2A A2B A2C A3A A3B A3C A4A A4B A4C M1A M1B M1C M2A M2B M2C M3A M3B M3C M4A M4B M4C
3 2 1 0 −1 −2 −3
experiment
infected
mock
time
1d
2d
3d
4d
descr
AP2/ERF
BBX
bHLH
GRAS
HD
MYB
NAC
WRKY
Terpenes
descr
MpMTPSL10
MpMTPSL2
MpMTPSL23
MpMTPSL3
MpMTPSL32
MpMTPSL6
MpMTPSL7
MpMTPSL8
experiment
time
Mapoly0034s0055
Mapoly0142s0043
Mapoly0825s0001
Mapoly0150s0003
Mapoly0034s0090
Mapoly0049s0062
Mapoly0034s0087
Mapoly0087s0087
descr
A1A A1B A1C A2A A2B A2C A3A A3B A3C A4A A4B A4C M1A M1B M1C M2A M2B M2C M3A M3B M3C M4A M4B M4C
3 2 1 0 −1 −2
experiment
infected
mock
time
1d
2d
3d
4d

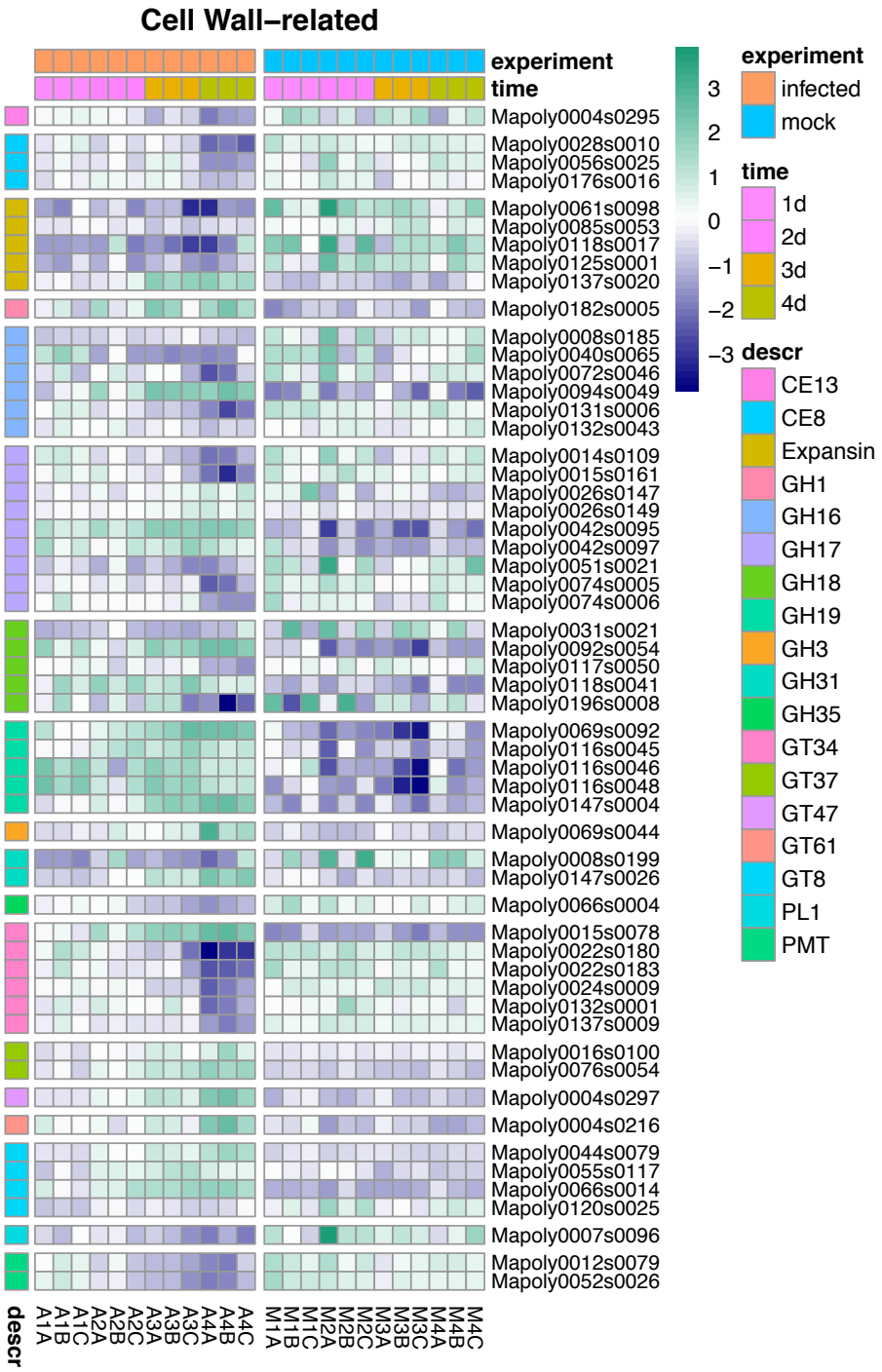
Cell Wall–related
experiment
time
Mapoly0004s0295
Mapoly0028s0010
Mapoly0056s0025
Mapoly0176s0016
Mapoly0061s0098
Mapoly0085s0053
Mapoly0118s0017
Mapoly0125s0001
Mapoly0137s0020
Mapoly0182s0005
Mapoly0008s0185
Mapoly0040s0065
Mapoly0072s0046
Mapoly0094s0049
Mapoly0131s0006
Mapoly0132s0043
Mapoly0014s0109
Mapoly0015s0161
Mapoly0026s0147
Mapoly0026s0149
Mapoly0042s0095
Mapoly0042s0097
Mapoly0051s0021
Mapoly0074s0005
Mapoly0074s0006
Mapoly0031s0021
Mapoly0092s0054
Mapoly0117s0050
Mapoly0118s0041
Mapoly0196s0008
Mapoly0069s0092
Mapoly0116s0045
Mapoly0116s0046
Mapoly0116s0048
Mapoly0147s0004
Mapoly0069s0044
Mapoly0008s0199
Mapoly0147s0026
Mapoly0066s0004
Mapoly0015s0078
Mapoly0022s0180
Mapoly0022s0183
Mapoly0024s0009
Mapoly0132s0001
Mapoly0137s0009
Mapoly0016s0100
Mapoly0076s0054
Mapoly0004s0297
Mapoly0004s0216
Mapoly0044s0079
Mapoly0055s0117
Mapoly0066s0014
Mapoly0120s0025
Mapoly0007s0096
Mapoly0012s0079
Mapoly0052s0026
descr
A1A A1B A1C A2A A2B A2C A3A A3B A3C A4A A4B A4C
M1A M1B M1C M2A M2B M2C M3A M3B M3C M4A M4B M4C
3 2 1 0 −1 −2 −3
experiment
infected
mock
time
1d
2d
3d
4d
descr
CE13
CE8
Expansin
GH1
GH16
GH17
GH18
GH19
GH3
GH31
GH35
GT34
GT37
GT47
GT61
GT8
PL1
PMT

Cuticle

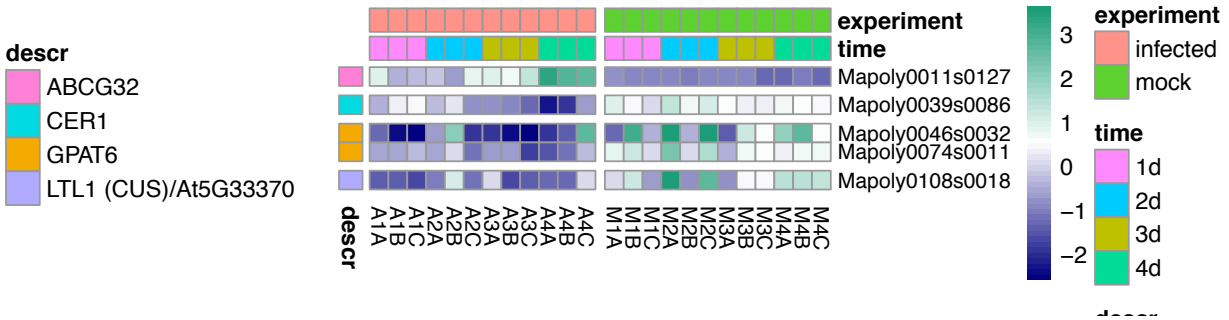

Abscisic Acid

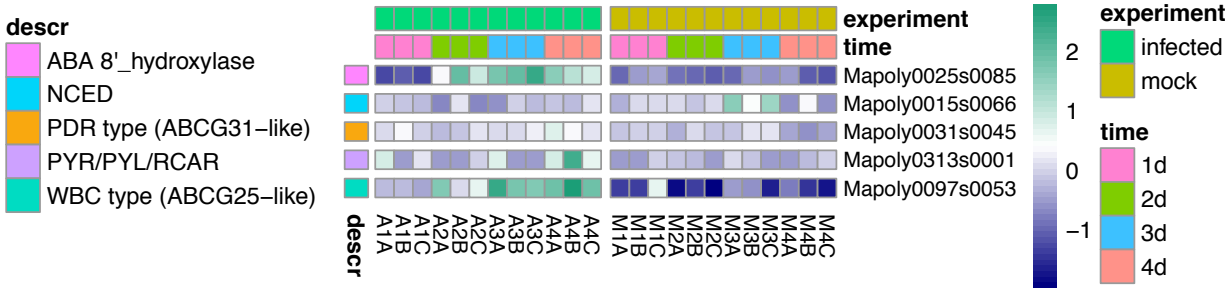

Auxin

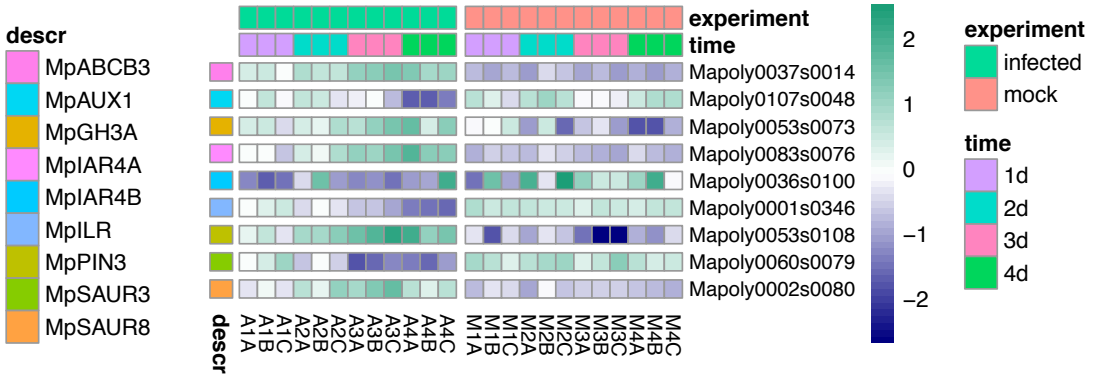

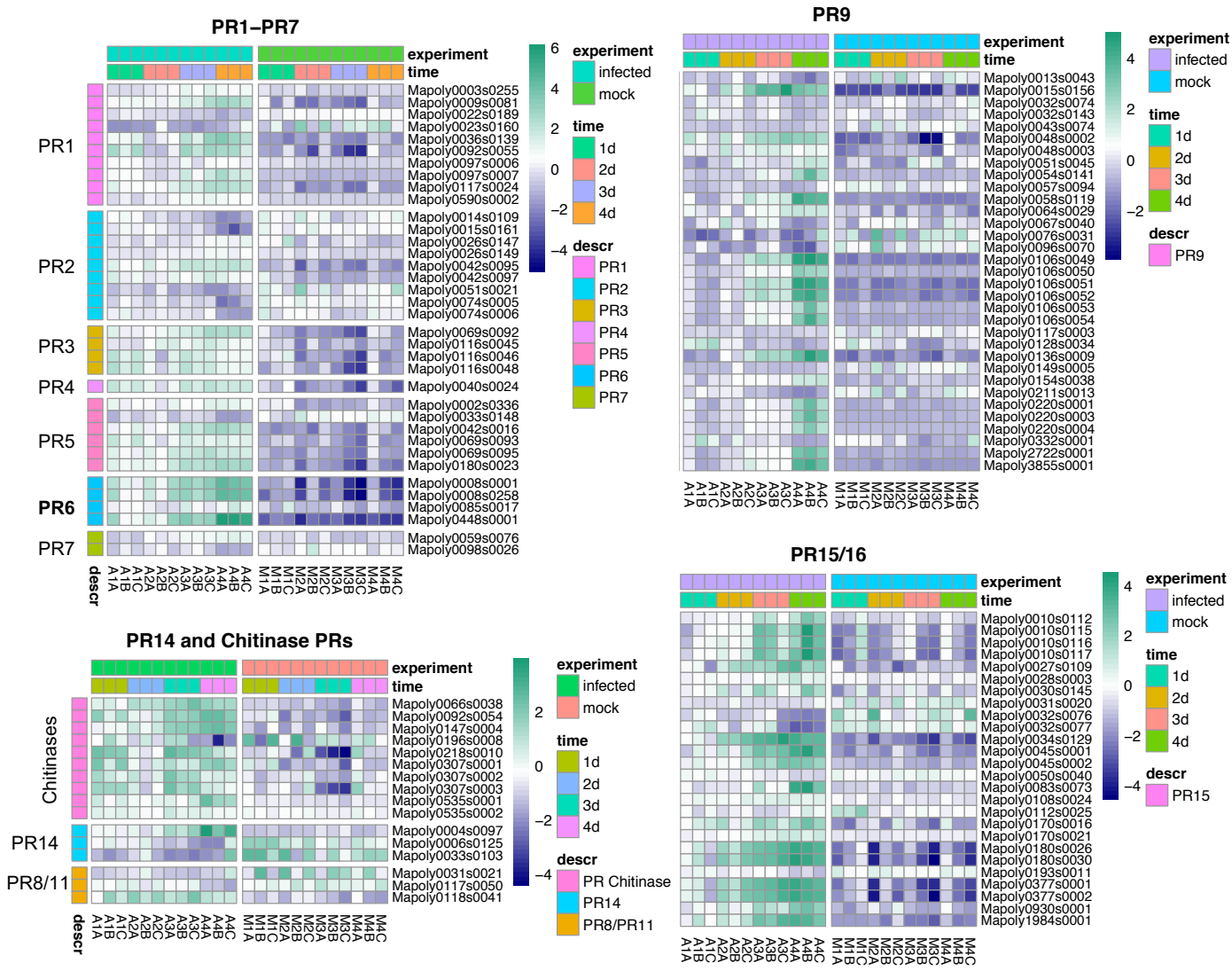

Figure S1. Heatmaps of PR gene candidate expression during the *Marchantia-Phytophthora* RNA-seq time-course, related to Figure 2 and Data S1

Heatmaps of annotated pathogenesis-related (PR) gene families were generated using vsd-stabilised counts from the *Marchantia-Phytophthora* RNA-seq time course data and display expression levels median-centered by gene. Time points represent 1, 2, 3, and 4 days post inoculation (d) of mock-inoculated (mock, water) or *P. palmivora*-treated (infected) *M. polymorpha* TAK1 plants

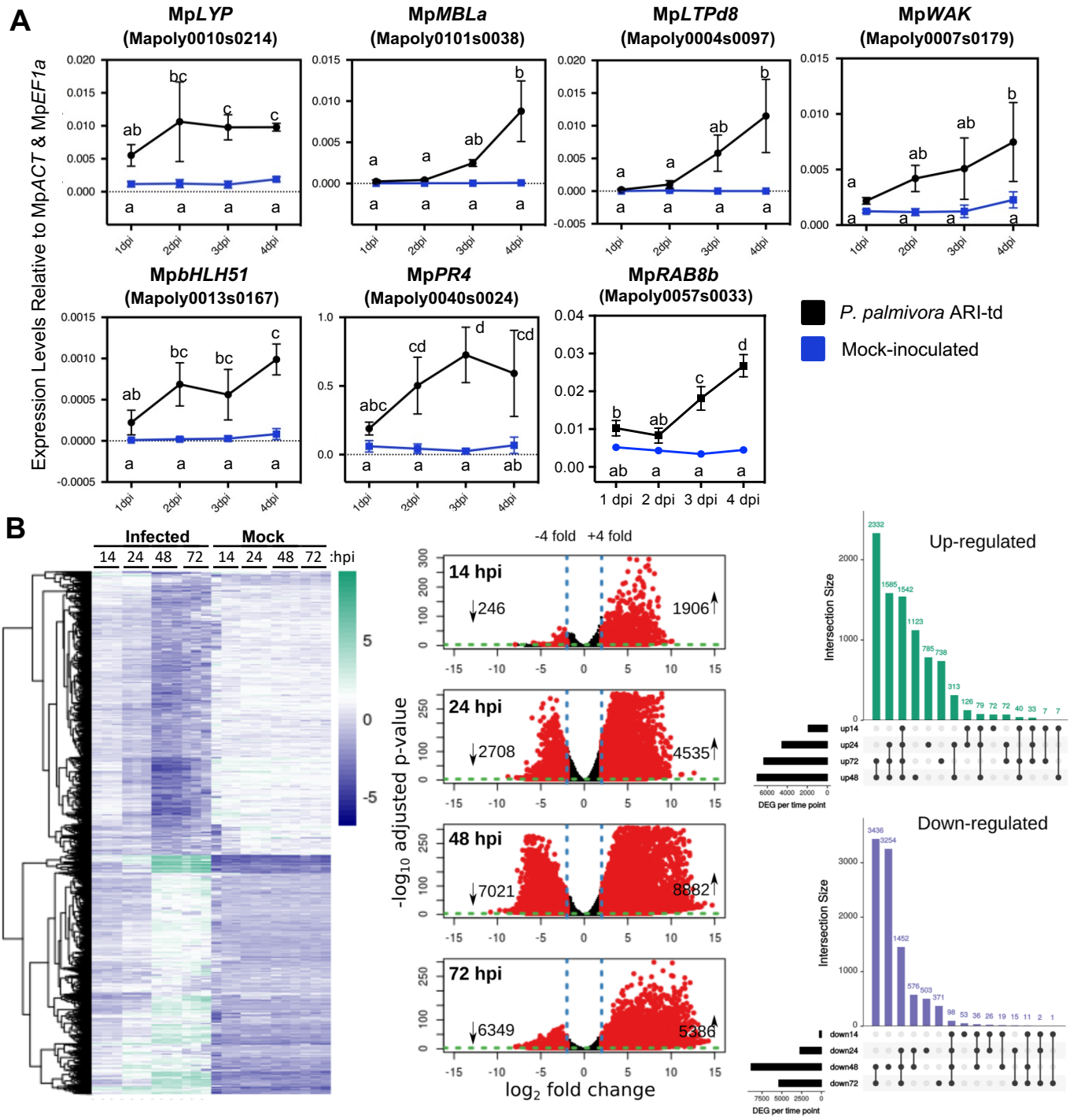

Figure S2. Extended analysis of *Marchantia-Phytophthora* and *Nicotiana-Phytophthora* RNA-seq data, related to Figure 3 and Data S1.

(A) qRT-PCR analysis of selected *Marchantia* DEGs identified from the *Marchantia-Phytophthora* RNA-seq analysis. Transcripts were quantified in mock-treated or *P. palmivora*-colonized (ARI-td) TAK1 plants from 1 to 4 days post inoculation (dpi). Expression values are shown relative to internal Mp*ACT* and Mp*EF1a* controls. Different letters signify statistically significant differences in transcript abundance (ANOVA, Tukey's HSD, P<0.05). (B) Overall statistics and characterization of the *Nicotiana benthamiana – Phytophthora palmivora* infection time course RNA-seq performed 14, 24, 48, and 72 hours post inoculation (hpi). The heatmap displays hierarchical clustering of significantly differentially expressed genes during *P. palmivora* infection (adjusted p-value $<10^{-3}$, log fold change ($|LFC| \geqslant 2$); variance-stabilised row-centered counts are shown. Volcano plots displaying pairwise differential expression analysis per time point. Significantly differentially expressed genes are displayed in red. Upset plots showing shared and time point-specific up-regulated and down-regulated *N. benthamiana* genes.

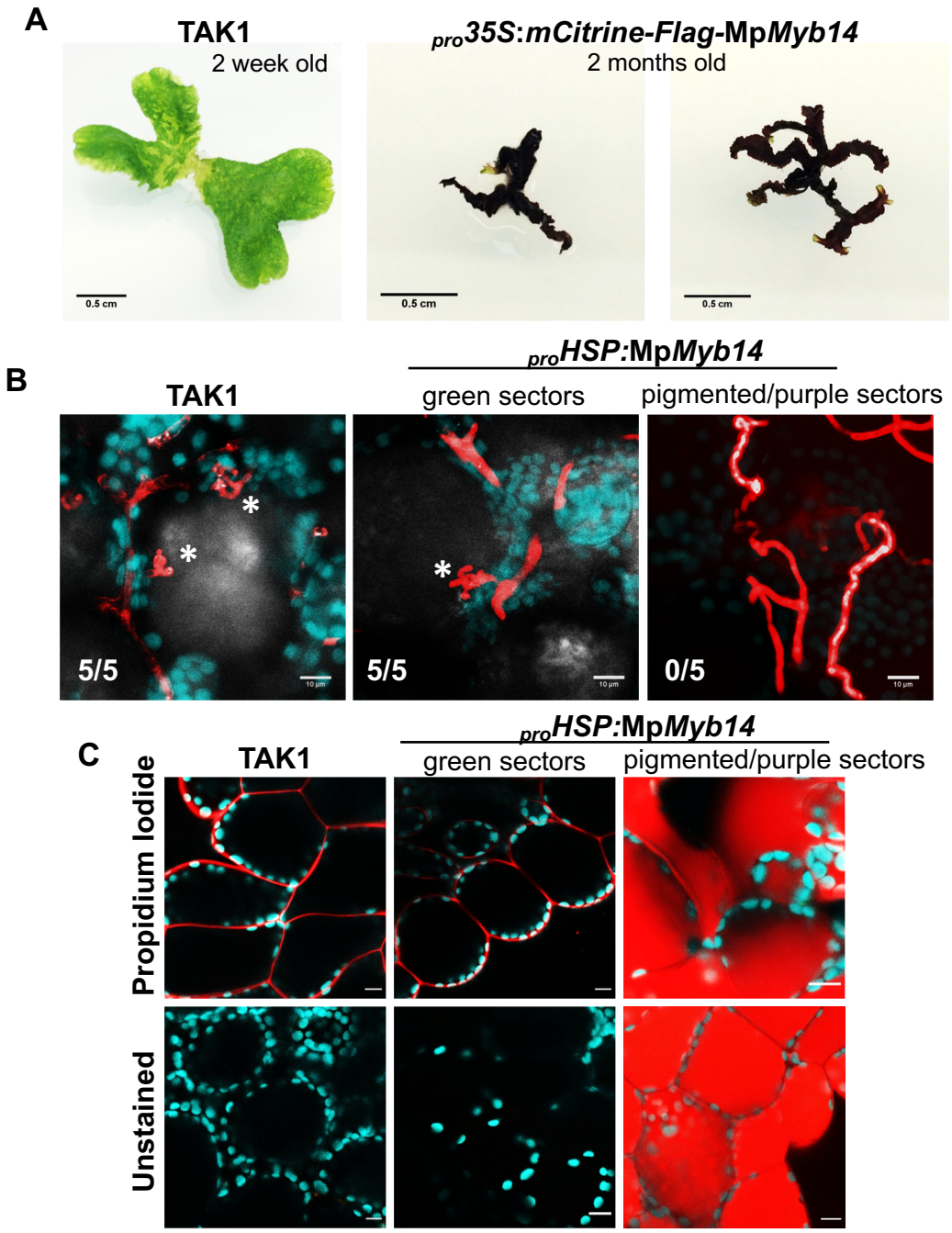

Figure S3. Morphological and microscopic analysis of pigment accumulation in *Marchantia, related to* Figure 6.

(A) Morphology of $_{pro}$*35S:mCitrine-Flag*-Mp*Myb14* transgenic lines. Bright-field images of wild-type TAK1 (2 weeks-old) compared to two independent transgenic $_{pro}$*35S:mCitrine-Flag*-Mp*Myb14*/TAK1 (2 months-old) lines. Scale bars = 0.5 cm. (B) Cellular infection dynamics in wild-type (TAK1) and non-pigmented (green sectors) compared to pigmented (purple sectors) $_{pro}$*HSP:*Mp*Myb14.* Images display red pathogen fluorescence (tdTomato) merged with plastid autofluorescence (cyan) and brightfield channels. Values indicate the number of independently infected individuals supporting at least one intracellular infection structure. Scale bars = 10 µm. Intracellular infection structures are denoted by an asterisk (*). (C) Propidium iodide (PI) staining to delineate cell membranes in wild-type and non-pigmented (green) compared to pigmented (purple) tissues of $_{pro}$*HSP:*Mp*Myb14* liverworts. Propidium iodided staining (red fluorescence) is overlaid with plastid autofluorescence (cyan). Pigment accumulation in $_{pro}$*HSP:*Mp*Myb14* lines overlaps with propidium iodide staining as indicated by observing unstained controls alongside PI-stained liverworts. Scale bars = 10 µm.

Primer Name	Sequence (5'-3')	Reference
Mp*ACT*-qF	AGGCATCTGGTATCCACGAG	[S1]
Mp*ACT*-qR	ACATGGTCGTTCCTCCAGAC	[S1]
Mp*EF1a*-qF	CCGAGATCCTGACCAAGG	[S1]
Mp*EF1a*-qR	GAGGTGGGTACTCAGCGAAG	[S1]
Pp*EF1a*-qF	CAAGATCCCGTTCGTGCCTA	[S2]
Pp*EF1a*-qR	GCGTTCAGGTTGTCAAGAGC	[S2]
Pp*Cdc14*-qF	TCTGCACGAGTTCCAGCATT	[S2]
Pp*Cdc14*-qR	CACCACTAGCGTCACGTTCT	[S2]
Mp*PAL*-qF	AATTCGCTGGGGCTCATTTC	[S3]
Mp*PAL*-qR	ACAGAGCGCAACCATGAAAG	[S3]
Mp*CHS*-qF	TTGAAAGCAACCCCGCTATG	[S3]
Mp*CHS*-qR	TGGGCGATGGCAATTTCTTG	[S3]
Mp*CHI-like*-qF	TCCTGCAACCATTCAAGTGC	[S3]
Mp*CHI-like*-qR	TGTCCTCACTGGCATACACAC	[S3]
Mp*C4H*-qF	TTGCCGAAAATGGGAATGCC	[S3]
Mp*C4H*-qR	TCAAGCAGCAGCATGTTCAC	[S3]
Mp*Myb14*-qF	TCGAAACTCTTCCACAGACAGA	This study
Mp*Myb14*-qR	GCTAATGAAGCCCGTACATAGG	This study
Mp*LYP*-qF	CTGATTCACCAAGCTCAGACAC	This study
Mp*LYP*-qR	AGTGCCAATCCAGTTTCTTCAT	This study
Mp*MBLa*-qF	CTCCTTCGATACGGACGGAA	This study
Mp*MBLa*-qR	GACTGGTCACTGGGGTTGTA	This study
Mp*LTPd8*-qF	TTCAGGTTCATCTCTCCATCCT	This study
Mp*LTPd8*-qR	CCCAGTCTGATTTTCATTTGGT	This study
Mp*WAK*-qF	CCGGAATCTCGTGAAATTGCT	This study
Mp*WAK*-qR	TGTGTTCGTCCAAATTGCCAT	This study
Mp*bHLH51*-qF	TGCGAAATCTGCACTGTTTACT	This study
Mp*bHLH51*-qR	ACAATTCCTCTAATCCGCTCAA	This study
Mp*PR4*-qF	TTCTGTGGTTTGCAGTTTCTTG	This study
Mp*PR4*-qR	CGCCATTGTAGTGATTCGTTAG	This study
Mp*Rab8b*-qF	GCCACGTCGTTCATCACTACÊ	This study
Mp*Rab8b*-qR	ATGGCTCCCCTGTAGTAAGC	This study

Table S1. Primers used in this study, related to STAR Methods Key Resources Table

Supplemental References

[S1] Saint-Marcoux, D., Proust, H., Dolan, L., and Langdale, J.A. (2015). Identification of Reference Genes for Real-Time Quantitative PCR Experiments in the Liverwort Marchantia polymorpha. PLOS ONE *10*, e0118678.

[S2] Le Fevre, R., O'Boyle, B., Moscou, M.J., and Schornack, S. (2016). Colonization of Barley by the Broad-Host Hemibiotrophic Pathogen *Phytophthora palmivora* Uncovers a Leaf Development–Dependent Involvement of *Mlo*. Molecular Plant-Microbe Interactions *29*, 385–395.

[S3] Kubo, H., Nozawa, S., Hiwatashi, T., Kondou, Y., Nakabayashi, R., Mori, T., Saito, K., Takanashi, K., Kohchi, T., and Ishizaki, K. (2018). Biosynthesis of riccionidins and marchantins is regulated by R2R3-MYB transcription factors in Marchantia polymorpha. Journal of Plant Research *131*, 849–864.

Graphical Abstract

Click here to access/download;Graphical Abstract;Carella-graphical-abstract2.jpg